Long-term progression of retinal degeneration in a preclinical model of CLN7 Batten disease as a baseline for testing clinical therapeutics

Ashley A. Rowe,[a] Xin Chen,[b,c] Emily R. Nettesheim,[a] Yacine Issioui,[a] Thomas Dong,[b] Yuhui Hu,[b] Souad Messahel,[c] Saima N. Kayani,[b,c,d,e] Steven J. Gray,[b,d,f,g,h] and Katherine J. Wert[a,c,f,g,*]

[a]Department of Ophthalmology, UT Southwestern Medical Center, Dallas, TX, 75390, USA
[b]Department of Pediatrics, UT Southwestern Medical Center, Dallas, TX, 75390, USA
[c]Peter O'Donnell Jr. Brain Institute, UT Southwestern Medical Center, Dallas, TX, 75390, USA
[d]Department of Neurology, UT Southwestern Medical Center, Dallas, TX, 75390, USA
[e]Children's Health, Children's Medical Center, Dallas, TX, 75390, USA
[f]Department of Molecular Biology, UT Southwestern Medical Center, Dallas, TX, 75390, USA
[g]Hamon Center for Regenerative Science and Medicine, UT Southwestern Medical Center, Dallas, TX, 75390, USA
[h]McDermott Center for Human Growth and Development, UT Southwestern Medical Center, Dallas, TX, 75390, USA

eBioMedicine
2022;85: 104314
Published Online XXX
https://doi.org/10.1016/j.ebiom.2022.104314

Summary

Background Batten disease is characterized by cognitive and motor impairment, retinal degeneration, and seizures leading to premature death. Recent studies have shown efficacy for a gene therapy approach for CLN7 Batten disease. This gene therapy approach is promising to treat cognitive and motor impairment, but is not likely to delay vision loss. Additionally, the natural progression of retinal degeneration in CLN7 Batten disease patients is not well-known.

Methods We performed visual examinations on five patients with CLN7 Batten disease and found that patients were far progressed in degeneration within their first five years of life. To better understand the disease progression, we characterized the retina of a preclinical mouse model of CLN7 Batten disease, through the age at which mice present with paralysis and premature death.

Findings We found that this preclinical model shows signs of photoreceptor to bipolar synaptic defects early, and displays rod-cone dystrophy with late loss of bipolar cells. This vision loss could be followed not only via histology, but using clinical live imaging similar to that used in human patients.

Interpretation Natural history studies of rare paediatric neurodegenerative conditions are complicated by the rapid degeneration and limited availability of patients. Characterization of degeneration in the preclinical model allows for future experiments to better understand the mechanisms underlying the retinal disease progression in order to find therapeutics to treat patients, as well as to evaluate these therapeutic options for future human clinical trials.

Funding Van Sickle Family Foundation Inc., NIH P30EY030413, Morton Fichtenbaum Charitable Trust and 5T32GM131945-03.

Copyright © 2022 The Author(s). Published by Elsevier B.V. This is an open access article under the CC BY-NC-ND license (http://creativecommons.org/licenses/by-nc-nd/4.0/).

Keywords: Neuronal ceroid lipofuscinoses; *Mfsd8*; Bipolar cell degeneration; Photoreceptor synapse; Electroretinography; Optical coherence tomography

Introduction

Death of the post-mitotic neuronal cells of the body have deleterious effects on health and viability, and are particularly harmful early in post-natal development. Neuronal ceroid lipofuscinoses (NCLs) are the most prevalent form of neurodegenerative disorders in paediatric patients, and most fall under diseases known collectively as Batten disease.[1,2] These are

*Corresponding author. Departments of Ophthalmology and Molecular Biology, UT Southwestern Medical Center, Dallas, TX, 75390, USA.
E-mail address: Katherine.Wert@UTSouthwestern.edu (K.J. Wert).

Research in context

Evidence before the study

Batten disease is characterized by death of the neuronal cells, such as those of the brain and retina. Patients show signs of disease as infants or young children, and these include movement impairment, neurological deficits, blindness and seizures, leading to premature death. Research studies have discovered the genes involved in Batten disease, although the precise mechanisms of action underlying the disease are not yet known. A recent study has found a gene therapy treatment that has moved forward to a clinical trial to treat the brain and spinal cord degeneration, but is not likely to treat the vision loss. The natural progression of vision loss needs to be understood in order to find and test therapeutic approaches for treatment in these patients.

Added value of this study

In this study, we performed visual examinations on five patients with CLN7 Batten disease and found that these patients are far progressed in vision loss in early childhood. To better define the disease progression, we examined the eyes of a preclinical mouse model of CLN7 Batten disease using both histological analysis as well as clinical imaging that is also performed in human patients. We found that the preclinical model showed early signs of synaptic defects, rod-cone photoreceptor degeneration, and late bipolar cell death, resulting in blindness.

Implications of all available evidence

The knowledge of the retinal cells affected during CLN7 Batten disease progression allows for therapeutics to be tested that target these specific cell types. Furthermore, our study has provided a baseline for CLN7 Batten disease vision loss that can be used when testing therapeutics in this preclinical model, to lead to future human clinical trials for treating vision loss associated with CLN7 Batten disease.

autosomal recessive disorders characterized by their age-of-onset to infantile, late-infantile, or juvenile Batten disease.[3–5] Patients present with cognitive and motor impairment, retinal dystrophy, and epileptic seizures that result in premature death.[1,3,6] In recent decades, studies have determined thirteen causal genes involved in Batten disease,[7] however there remains a critical need to understand the definitive functions of these genes to provide better therapeutic outcomes for patients.

Currently, there are no available treatments to alleviate clinical symptoms for the majority of Batten disease.[8,9] In the case of CLN2 Batten disease, research studies have shown that a recombinant human tripeptidyl peptidase-1 (TPP1) can be delivered into the cerebrospinal fluid every two weeks.[10–13] While positive results have been seen with this form of enzyme replacement therapy, it has a high incremental cost-utility ratio and the frequent delivery causes distress for paediatric patients.[14] As Batten disease is monogenic and caused by recessive inheritance, gene therapy vectors are a promising treatment approach. Recently, a clinical trial has emerged to test the delivery of gene therapy for the treatment of CLN7 Batten disease (NCT04737460).

The CLN7 form of Batten disease is caused by more than thirty-five mutations in the major facilitator superfamily domain containing 8 (*MFSD8*) gene, leading to protein reduction, or an inactive form of the CLN7 protein.[15,16] Clinical signs of disease present during the late-infantile stage, with most patients dying in late childhood to teenaged years.[17] In addition, some compound heterozygous patients have been identified with late-onset disease characterized by retinal dystrophies, including non-syndromic macular dystrophies with central cone involvement.[7] Although this new gene therapy approach shows promise, it is not expected to pass the blood-retina barrier to efficiently prevent retinal degeneration in these CLN7 patients.

Studies are needed that examine the efficiency and efficacy of this gene therapy vector, or other potential therapeutic approaches, on retinal degeneration for CLN7 Batten disease. In order to examine the therapeutic efficiency and efficacy, there need to be phenotypic outcomes that can be monitored with and without treatment. Thus, an understanding of the natural progression of retinal degeneration in these patients is necessary. In this study, we performed visual examinations and clinical imaging on five patients with CLN7 Batten disease. We found that patients were far progressed in retinal degeneration within their first five years of life. Therefore, we utilized a preclinical model of CLN7 Batten disease and characterized the long-term progression of retinal degeneration. Along with the rod degeneration detectable early in disease that replicated the histological findings previously published,[18] we found a possible defect in photoreceptor to bipolar cell synaptic connectivity, early loss of both rod and cone function, and a loss of the inner nuclear layer (INL) at late stages of disease. The ability to follow the

degeneration using clinical imaging in this preclinical model provides testing outcomes that can be used to monitor the potential efficacy of therapeutic approaches to treat retinal degeneration caused by CLN7 Batten disease.

Methods

Human patients

Patients were enrolled in one of two Institutional Review Board (IRB)-approved clinical studies at the Children's Research Hospital and the University of Texas Southwestern Medical Center (UTSW; see Ethics). Patient I is a female that underwent clinical evaluation at four years and two months of age. She is compound heterozygous for an early stop mutation (c.1444C>T) and frameshift mutation (c.1206del) in *MFSD8*. Patient II is a male that underwent clinical evaluation at four years and eight months of age. He carries a homozygous missense mutation (c.1373C>A) in *MFSD8*. Patient III is a female that underwent clinical evaluation at five years and two weeks of age. She carries a homozygous early stop mutation (c.103C>T) in *MFSD8*. Patient IV is a female that underwent clinical evaluation at five years and eleven months of age. She carries a homozygous splice donor mutation (c.198+2T>C) in *MFSD8*. Patient V is a male that underwent clinical evaluation at six years and eleven months of age. He is compound heterozygous for a frameshift mutation (c.1036delG) and a splice acceptor mutation (c.440-2A>T) in *MFSD8*. See Table 1 for more details. The normal control patient was eighteen years of age at clinical evaluation and presented with intracranial hypertension but normal retinal function and no known mutations in *MFSD8*.

Patient imaging

Visual acuity exams were attempted with variations of method based on the communication ability of the patients. Electroretinography (ERG) was conducted in accordance with international standards set by the International Society for Clinical Electrophysiology of Vision (ISCEV) and recorded on a Diagnosys Espion Electrophysiology System (Diagnosys LLC, Littleton, MA, USA). Recordings for scotopic ERG with a flash intensity of 3.0 Hz were followed by photopic ERG with a flash intensity of 3.0 Hz. Optical coherence tomography (OCT) was attempted using the Heidelberg HRA/OCT Spectralis (Heidelberg Engineering, Heidelberg, Germany).

Mouse lines and husbandry

Mfsd8 knockout (KO) mice (RRID: MGI:6388452) were obtained, carrying a deletion of exon 2 as previously described.[19,20] Heterozygous *Mfsd8* mice were bred to obtain litters of wild-type, heterozygous, and homozygous *Mfsd8* KO mice, herein referred to as wild-type, *Cln7* heterozygous, or *Cln7* KO, respectively. C57BL/6J mice (Jackson Laboratory, Bar Harbor ME; RRID: MSR_JAX:000664) were used as additional controls. Euthanasia was performed by cervical dislocation or CO_2 asphyxiation followed by secondary cervical dislocation. All mice were maintained in approved animal facilities at the UTSW and were kept on a normal light–dark cycle (12/12 h). Food and water were available *ad libitum* throughout the experiment.

Retinal histology and quantification

Mice were sacrificed, and the eyes enucleated and processed as previously described.[21,22] Quantification of retinal nuclei in either the outer nuclear layer (ONL) or inner nuclear layer (INL) was conducted on several sections that contained the optic nerve, as follows: the distance between the optic nerve and ciliary body was divided into three, approximately equal, regions on each side of the retina. The number of nuclei in four columns were

Patient ID	Gender	Age of testing	Affected gene	Mutation information	Zygosity	Predicted DNA variation
I	Female	4 years, 2 months	*MFSD8*	c.1444C>T (p.Arg482Ter) c.1206del (p.Ile403LeufsTer11)	Compound Heterozygous	Stop gained Frameshift
II	Male	4 years, 8 months	*MFSD8*	c.1373C>A (p.Thr458Lys)	Homozygous	Missense
III	Female	5 years, 0.5 months	*MFSD8*	c.103C>T (p.Arg35Ter)	Homozygous	Stop gained
IV	Female	5 years, 11 months	*MFSD8*	c.198+2T>C	Homozygous	GT Splice donor
V	Male	6 years, 11 months	*MFSD8*	c.1036delG (p.Val346LeufsTer68) c.440-2A>T	Compound Heterozygous	Frameshift Splice acceptor

C, cytosine; T, thymine; A, adenine; G, guanine; Arg, arginine; Ter, termination; Ile, isoleucine; Leu, leucine; Thr, threonine; Lys, lysine; Val, valine; Fs, frameshift. A summary of the genetic variants in five CLN7 Batten disease patients along with their age at time of testing and gender. "c" denotes the change at the nucleotide level, and "p" denotes the change at the amino acid level, where applicable.

Table 1: **Human CLN7 patient variants.**

counted within each region. These counts were used to determine the average thickness of the ONL and INL for each individual animal and within each region of the retina, spanning from the ciliary body to the optic nerve head (ONH) and back out to the ciliary body. Each section contained upper and lower retina as well as the posterior pole. N = five eyes per group and five sections per eye were used for analysis. Statistics were performed with a multiple comparisons test with Holm-Šidák's correction.

Immunohistochemistry (IHC)

Mouse eyes were prepared and sectioned for IHC as previously described.[21] Primary antibodies were GFAP (1:500, catalog Mab360, MilliporeSigma, RRID: AB_11212597), PSD95 (1:100, catalog ab238135, Abcam, RRID: AB_2895158), Red/Green Opsin (1:250, catalog AB5405, MilliporeSigma, RRID: AB_177456), PKCα (1:250, catalog sc8393, Santa Cruz Biotech, RRID: AB_628142), Blue Opsin (1:250, catalog AB5407, MilliporeSigma, RRID: AB_177457), Glutamine Synthetase (1:250, catalog MA5-27749, Invitrogen, RRID: AB_2735204), RBPMS (1:250, catalog ab152101, Abcam, RRID: AB_2923082), IBA1 (1:500, catalog ab178846, Abcam, RRID: AB_2636859) and VGLUT1 (1:250, catalog 48-2400, Thermo Fisher Scientific, RRID: AB_2533843). Secondary antibodies were Goat anti-Mouse Alexa Fluor 488 (1:1000, catalog A11001, Thermo Fisher Scientific, RRID:AB_2534069) and Goat anti-Rabbit Alexa Fluor 594 (1:1000, catalog A11012, Thermo Fisher Scientific, RRID:AB_2534070). Slides were imaged on a Leica SP8 laser scanning confocal microscope using a 25× water immersion objective lens or a 63× oil immersion objective lens. N = three mice and three or more sections per eye were used for analysis.

Western blotting

Retina tissue was collected as previously described.[21,22] Samples represent both the left and right retinas from a mouse combined. Samples were lysed in RIPA buffer (Thermo Fisher Scientific, catalog 89900) with protease and phosphatase inhibitor added (Thermo Fisher Scientific, catalog 87786). During lysis, samples were sonicated in 5 s pulses a total of three times. Analysis was performed by running samples on either a 4–12% Bis-Tris gradient gel (Thermo Fisher Scientific, NW04125BOX) or a 3–8% Tris Acetate Gel (Thermo Fisher Scientific, EA03755BOX) and then transferred to a nitrocellulose membrane using the iBlot2 dry transfer system (Thermo Fisher Scientific, IB21001). Transfer was done in a three-step sequence: 20 V for 1 min, 23 V for 4 min, and 25 V for 2 min. Following transfer, membranes were blocked for 1 h at room temperature in 5% milk in TBST. Primary antibodies were diluted in 5% BSA in TBST and placed on the membrane and left shaking in a 4 °C fridge overnight. Primary antibodies were: PSD95 (1:2000, catalog ab238135, Abcam, RRID: AB_2895158), Red/Green Opsin (1:1000, catalog AB5405, MilliporeSigma, RRID: AB_177456), PKCα (1:1000, catalog sc8393, Santa Cruz Biotech, RRID: AB_628142), Blue Opsin (1:1000, catalog AB5407, Millipore Sigma, RRID: AB_177457), RBPMS (1:250, catalog ab152101, Abcam, RRID: AB_2923082), IBA1 (1:500, catalog ab178846, Abcam, RRID: AB_2636859), VGLUT1 (1:1000, catalog 48-2400, Thermo Fisher Scientific, RRID: AB_2533843), PROX1 (1:2000, catalog AB5475, Millipore Sigma, RRID: AB_177485), and GAPDH (1:2000, catalog GTX82560, GeneTex, RRID: AB_11174663). The next day, the membranes were washed three times in TBST followed by a 45 min incubation in secondary antibodies (LICOR, catalog 926-32211, RRID: AB_621843; catalog 926-68070, RRID: AB_10956588) diluted in 5% milk-TBS. Membranes were then washed three times in TBST, followed by one wash in TBS. Membranes were kept protected from light during the antibody staining process once secondary antibody had been added. Imaging and quantification were performed using the LI-COR Odyssey CLx. N = three mice and at least two technical replicates per mouse per antibody were used for analysis. Statistics were performed with one-way ANOVA with Tukey's multiple comparisons test.

Retinal imaging

Infrared (IR) and autofluorescence (AF) imaging were obtained with the Spectralis OCT scanning laser confocal ophthalmoscope (OCT-SLO Spectralis; Heidelberg Engineering, Franklin, MA, USA) as previously described.[21–26] Images were taken with a 55-degree wide focus lens (Heidelberg Engineering). The optic nerve was positioned in the centre of the image and 100 image sweeps were averaged to obtain the composite. For OCT, the IR image was used to select a plane through the centre of the eye, transecting the ONH. OCT images were taken by averaging one hundred image sweeps. N ≥ five mice per group.

OCT retinal thickness measurements

For each experimental group and time point, five mouse eyes from separate mice were analysed for changes in OCT retinal thickness. The measurements were taken at six regions, three on each side of the optic nerve (Fig. S1). The first location was determined as being the closest to the optic nerve. A second location was located at the outer edge of the image and the third measurement was taken at the halfway point between the first two locations. Thickness of the neural retina was measured from the retinal nerve fiber layer (RNFL) to the retinal pigmented epithelium (RPE). Measurements were taken in micrometers using the Heidelberg Eye

Explorer Software (Franklin, MA, USA). Statistics were performed with two-way ANOVA with Tukey's multiple comparisons test.

Electroretinography (ERG)

Scotopic ERG recordings were collected as previously described.[21,22] Briefly, mice were dark-adapted for at least 12 h, manipulations were conducted under dim red-light illumination, and recordings were made using either the Celeris ERG system by Diagnosys LLC (Lowell, MA, USA) or the Phoenix MICRON Ganzfeld ERG System (Phoenix Technology Group, Pleasanton, CA, USA). On the Ganzfeld ERG, retinal responses were recorded at four different green light intensity settings: –1.7, –1.1, 1.9, and 2.5 log cd.s/m^2. On the Celeris ERG, retinal responses were recorded at three different white light intensity settings: 0.01, 0.1 and 1.0 cd.s/m^2. A minimum of seven measurements were recorded and averaged for each light setting. Photopic ERG was recorded using the Celeris ERG by first exposing the mouse eyes to 10 min of white light, followed by flashes at two white light settings: 3.0 and 10.0 Hz, each one averaging at least fifteen sweeps. Flicker response was measured at 10 Hz and 30 Hz, each averaging fifty sweeps. N ≥ eight eyes per group. Statistics were performed using two-way ANOVA with Šidák's multiple comparisons test, one-way ANOVA with Tukey's multiple comparisons test, or unpaired student's *t*-test (see Results and Figure Legends for specific details).

Pattern ERG (PERG) and visually evoked potentials (VEP)

Mice were dark adapted for 12 h before eyes were dilated and animals were anesthetized via an IP injection of anaesthesia [1 mL ketamine 100 mg/mL (Ketaset III, Fort Dodge, IA, USA) and 0.1 mL xylazine 20 mg/mL (Akorn Inc., Lakeforest, IL, USA) in 8.9 mL PBS]. PERG and VEP recordings were taken simultaneously with a PERG stimulator on one eye, a second eye used as a corneal ground reference and additional electrodes in the forehead, cheek, and tail. Six hundred sweeps were averaged. N = five mice per group. Statistics were performed using the unpaired student's *t*-test.

Statistical analysis

Data are reported as mean ± SEM unless otherwise noted. GraphPad Prism Software (version 9.0) was used to generate graphs and perform statistical analysis. We calculated the sample sizes based on an effect size of 1 with standard deviation (SD) of 0.5. This calculation was based on our previously published work with mouse models of retinal degeneration using similar experimental methods. For example, for live imaging, this was based on an SD of 50 μV when looking for an effect of 100 μV, or during late degeneration an SD of 10 μV when looking for an effect of 20 μV. This indicated a sample size of approximately four mice to achieve 80% power when significance is set to $P < 0.05$ to compare two groups with two-tailed *t*-test. For the precise calculation, we used the formula: sample size = $2SD^2(1.96 + 0.842)^2/d^2$. We did increase our mouse number used for the majority of our experimental methods, to ensure that we had an appropriate number of mice of both sexes and littermates from more than one litter included in the data results. Data comparing two groups were analysed via two-tailed *t*-test. Data comparing more than two groups were analysed using one-way ANOVA followed by Tukey's post-hoc multiple comparison's test. Data comparing two groups over multiple time points were analysed using multiple two-tailed *t*-tests with the Holm-Šidák's method to correct for multiple comparisons. Data with two independent variables were analysed using two-way ANOVA followed by Tukey's post hoc multiple comparison's test. Normal distribution and homogeneity of variance was determined by graphical analysis. See individual methods sections, results and figure legends for specific testing methods. No mice were excluded from the analysis. A P value of less than 0.05 was considered significant and measurements were done blinded to experimental groups (i.e. genotypes).

Ethics

The study protocol was approved by the IRB for Human Subjects Research at UTSW (STU#2020-0640 and #2018-0226), was HIPAA compliant, and adhered to the tenets of the Declaration of Helsinki. Informed consent was obtained prior to any study procedures starting. Parents consented for their children to participate, and no assent was obtained as children were below the age of 10 years. Informed consent was written consent. All animal experiments were performed in accordance with the ARVO Statement for the Use of Animals in Ophthalmic and Visual Research and were approved by the Animal Care and Use Committee at UTSW (APN#2019-102840).

Role of funders

P30 EY030413 for the Department of Ophthalmology at UTSW was used to support the running of equipment under the Microscopy and Digital Imaging Module. Partial support for the project was provided by a kind gift to SJG from the Morton Fichtenbaum Charitable Trust. No other funding source had any roles in this project. No funding source had any role in study design, data collection, data analyses, data interpretation, or the writing of the manuscript.

Results

Visual deterioration in human patients with CLN7 Batten disease

Five patients carrying homozygous or compound heterozygous mutations in *MFSD8* that were pathogenic for CLN7 Batten disease underwent visual examination and clinical imaging (Table 1). During testing of visual acuity, three out of five patients were uncooperative and no results were able to be obtained by the clinician. Patient III completed fix and follow examination. Patient I completed an LEA symbol examination which showed a reduction in visual acuity (Table 2).

Scotopic and photopic electroretinography (ERG) was performed to test for retinal function. Difficulty in patient cooperation led to artifacts and noise upon ERG analysis, with Patient III unable to continue photopic testing due to elevated distress (Fig. 1). However, all ERG results displayed a loss in visual function for each patient (Fig. 1). Interestingly, Patient I - the youngest in the study - displayed an electronegative scotopic ERG with detectable, but reduced, a-wave OU (141.3 μV OD and 197.9 μV OS) at a 3.0 Hz flash intensity that was also detected at 10 Hz.

Optical coherence tomography (OCT) was attempted in all five patients. Due to the inability for patients to cooperate, no reliable OCT images were obtained for either eye (Table 2). Thus, reliance on clinical imaging to characterize retinal degeneration in patients with CLN7 Batten disease is not ideal. However, determining the phenotypic progression of retinal neurodegeneration in CLN7 Batten disease is necessary for understanding the natural history of disease to be able to define the potential efficacy of clinical therapeutics.

Long-term analysis of retinal degeneration in a preclinical model of CLN7 Batten disease

To address this critical need, we utilized an available preclinical model for CLN7 Batten disease: the *Mfsd8* knockout (KO) mouse model.[7] The *Cln7* KO mouse has previously been shown to have rod degeneration through four months of age.[18] Additionally, this preclinical model was used to provide efficacy of intrathecal gene therapy injections, leading to the onset of a human clinical trial for CLN7 Batten disease patients[20] (NCT04737460). However, this preclinical mouse model did not display detectable loss of the cone photoreceptors or bipolar cells in the four month period of analysis.[18]

It is possible that the loss of additional retinal cells occurs after four months of age in the *Cln7* KO mice. Therefore, we characterized the progression of retinal degeneration via histological analysis through six months of age, the time in which the mice present with seizures, neurological degeneration, and premature death.[20] As expected for the recessive inheritance, heterozygous *Cln7* mice displayed similar retinal morphology compared to wild-type controls at six months of age (Fig. 2a). Quantification of the outer nuclear layer (ONL; Fig. 2b) and inner nuclear layer (INL; Fig. 2c) showed no significant differences between wild-type (black) and heterozygous *Cln7* mice (blue) [Multiple comparisons test with Holm-Šidák's correction].

In contrast, the *Cln7* KO mice displayed a loss of the ONL beginning at one month of age, with rapid degeneration between one and two months of age, and continuing to decline through six months of age (Fig. 2d). Quantification of ONL thickness showed a significant reduction (approximately 50–65% depending on the region of the retina examined based on distance from the optic nerve head) in the *Cln7* KO mice (orange) compared to heterozygous controls (blue) at three months of age (Fig. 2e) [$P < 0.0001$; multiple comparisons test with Holm-Šidák's correction]. No significant differences were noted in the INL thickness between the *Cln7* KO mice and heterozygous controls at three months of age (Fig. 2f), similar to previously published research[18] [Multiple comparisons test with Holm-Šidák's correction]. However, at six months of age, *Cln7* KO mice not only had lost approximately 82–89% of ONL thickness of heterozygous controls (Fig. 2g), but also had a significant - approximately 37% - loss of INL thickness (Fig. 2h) [***$P = 0.00018$ and $P = 0.00017$;

Patient ID	OCT imaging	ERG	Visual acuity
I	Uncooperative	Electronegative, reduced signal	LEA symbols; 20/125 OS, 20/200 OD
II	Uncooperative	Uncooperative, attempted. Reduced signal	Unable to comply
III	Uncooperative	Uncooperative, attempted. Reduced signal	Unable to fix and follow
IV	Uncooperative	Uncooperative, attempted. Reduced signal	Unable to comply
V	Uncooperative	Not tested	Unable to comply

OS, left eye; OD, right eye; OCT, optical coherence tomography; ERG, electroretinography. Five CLN7 Batten disease patients were examined for visual acuity and retinal health with results summarized in this table. "Uncooperative" denotes that examination was stopped or produced data with artifacts due to patient distress. "Unable to comply" denotes the patient was unable to perform the necessary communication and understanding required for the visual acuity test.

Table 2: **Summary of human CLN7 patient visual examinations.**

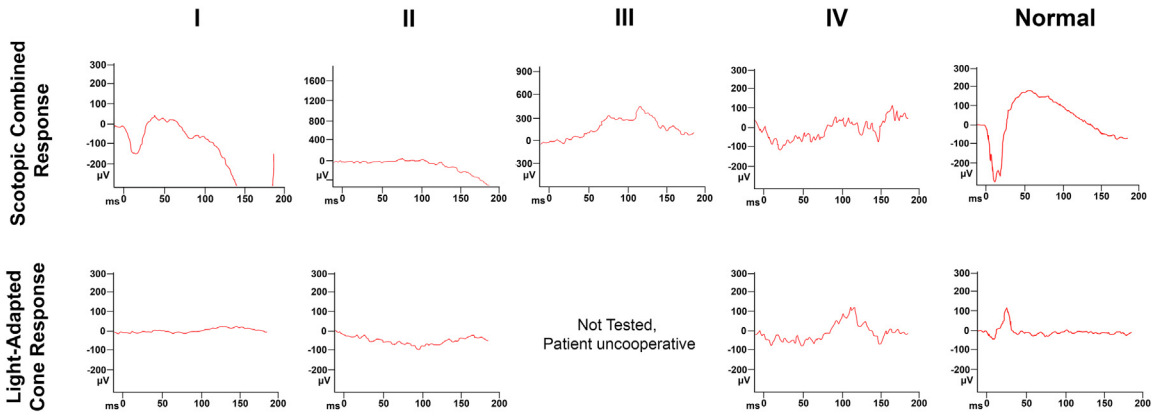

***Fig. 1:* Severe loss of visual function in human patients with CLN7 Batten disease**. Average electroretinography (ERG) traces for patients I–IV (see Table 1) and a normal control patient for the dark-adapted, scotopic combined response (top row) and light-adapted, cone response (bottom row). Light intensities were 3.0 Hz.

****P < 0.0001; multiple comparisons test with Holm-Šidák's correction]. This is the first time that the loss of the INL, similar to that seen in human CLN7 Batten disease patients, has been shown in this mouse model.

Reduction in the bipolar cells and photoreceptor synapses by five months of age in the *Cln7* KO mouse

To investigate these changes further, we examined the *Cln7* KO retinas at early- (two months) and late- (five months) stages of disease compared to wild-type controls (Fig. 3). As expected, the *Cln7* KO mice showed elevated glial activation by immunostaining for glutamine synthetase (GS) and glial fibrillary acidic protein (GFAP) at both two and five months of age, indicative of retinal stress during both the early- and late-stages of disease (Fig. 3; Fig. S2). Microglial activation was also elevated at both the early- and late-stages of disease in the *Cln7* KO mice compared to wild-type controls, and ionized calcium-binding adaptor molecule 1 (IBA1) protein was found to be significantly elevated in the *Cln7* KO mice compared to controls upon Western blot analysis (Figs. 3 and 4; Fig. S2) [**P = 0.0032 for comparison to two month wild-type and 0.0028 for comparison to five month wild-type; ****P < 0.0001; one-way ANOVA with Tukey's multiple comparisons test].

No change was noted for the retinal ganglion cells, either by immunostaining or Western blot analysis for RNA binding protein with multiple splicing (RBPMS; Figs. 3 and 4; Fig. S3) [One-way ANOVA with Tukey's multiple comparisons test]. The bipolar cells, stained with protein kinase c alpha (PKCα), appeared similar between wild-type and early-stage *Cln7* KO mice upon immunostaining analysis (Fig. 3; Fig. S3). There was a slight significant elevation in PKCα between five month wild-type and two month *Cln7* KO retinas with Western blot analysis (Fig. 4) [*P = 0.013; one-way ANOVA with Tukey's multiple comparisons test]. However, there was a thinning of the bipolar cell layer present by late-stage of disease in the *Cln7* KO mice (Fig. 3; Fig. S3), as would be expected with the reduction in INL thickness seen at six months of age (Fig. 2h). Western blot analysis of PKCα showed a significant decline between the early- and late-stage *Cln7* KO mice, although it did not show significance against the wild-type controls (Fig. 4) [**P = 0.0038; one-way ANOVA with Tukey's multiple comparisons test]. This trend was also detected, without significance, by examining prospero homeobox 1 (PROX1) protein, which represents the amacrine cells as well as some bipolar and horizontal cells of the INL (Fig. 4) [One-way ANOVA with Tukey's multiple comparisons test].

Since Patient I indicated that there may be a defect in photoreceptor to bipolar synaptic signalling prior to the loss of phototransduction (Fig. 1), we examined the wild-type and *Cln7* KO retinas for synaptic markers (Fig. 3). Interestingly, post-synaptic density protein-95 (PSD95) in the outer plexiform layer (OPL) appeared similar between early-stage *Cln7* KO mice and wild-type controls, even though ONL thickness is severely reduced by this time (Fig. 3; Fig. S4). However, Western blot analysis did show a significant loss of PSD95 in the early-stage *Cln7* KO mice compared to wild-type controls (Fig. 4) [P < 0.0001; one-way ANOVA with Tukey's multiple comparisons test]. At late-stage, a reduction in PSD95 was detectable via immunostaining in the *Cln7* KO mice, likely reflecting the loss of the photoreceptors. This was also significant upon protein analysis (Fig. 4) [P < 0.0001; one-way ANOVA with Tukey's multiple comparisons test]. Vesicular glutamate transporter 1 (VGLUT1) is known to

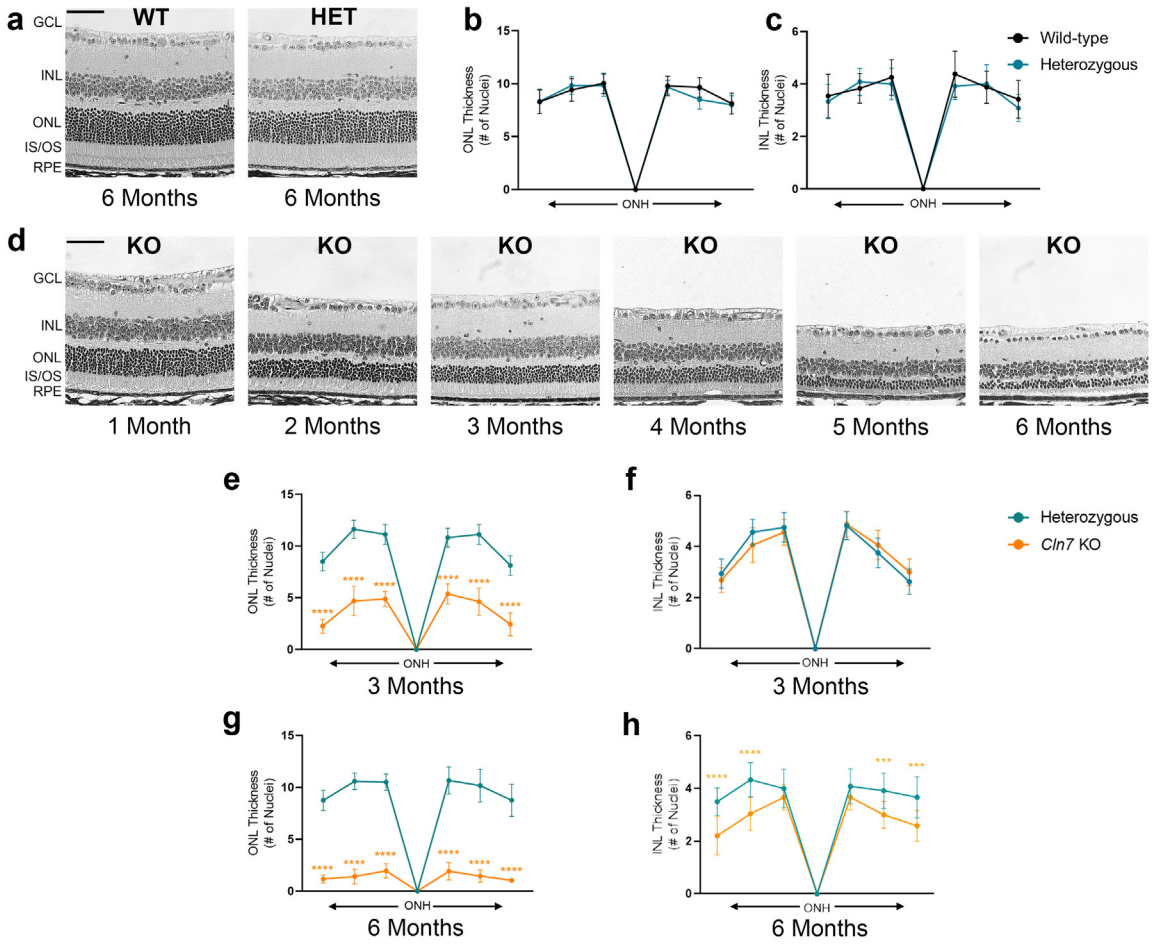

***Fig. 2:* Significant loss of the outer nuclear layer (ONL) and inner nuclear layer (INL) during progression of retinal degeneration in the *Cln7* knockout (KO) mouse model**. (a) Representative hematoxylin and eosin (H&E)-stained sections from a wild-type (left) and a *Cln7* heterozygous (right) mouse eye at six months of age. Spider plot quantification of (b) ONL thickness and (c) INL thickness at six different regions of wild-type (black) and *Cln7* heterozygous (teal) mice at six months of age. (d) Representative H&E-stained sections from *Cln7* KO mice monthly through six months of age. Spider plot quantification of three month *Cln7* heterozygous (teal) and *Cln7* KO (orange) mice for (e) ONL thickness and (f) INL thickness. Spider plot quantification of six month *Cln7* heterozygous (teal) and *Cln7* KO (orange) mice for (g) ONL thickness and (h) INL thickness. N = five eyes per group and five sections per eye. GCL, ganglion cell layer; IS/OS, inner segment/outer segment; RPE, retinal pigmented epithelium; ONH, optic nerve head. Scale bar = 50 µm. Error bars = SD. Multiple comparisons test with Holm-Šidák's correction. ***P = 0.00018 and P = 0.00017; ****P < 0.0001.

be required by the photoreceptors to signal to the second- and third-order neurons of the retina, such as the bipolar cells.[27–29] We found that there is a slight reduction in VGLUT1 at the OPL, but not the inner plexiform layer (IPL), early in the *Cln7* KO mice compared to controls. However, Western blot analysis of the early-stage *Cln7* retinas showed a slight elevation of VGLUT1 compared to wild-type controls (Fig. 4) [P = 0.028; one-way ANOVA with Tukey's multiple comparisons test]. VGLUT1 was still present in both the OPL and IPL at late-stage of disease with no significant changes (Figs. 3 and 4; Fig. S4) [One-way ANOVA with Tukey's multiple comparisons test].

Long-term clinical imaging indicates progressive photoreceptor degeneration in the *Cln7* KO mice

In order to establish a natural history of retinal degeneration in the *Cln7* KO mice that would provide a baseline to test clinical therapeutics, we performed clinical imaging over six months in the wild-type, *Cln7* heterozygous, and *Cln7* KO mice. Infrared (IR) and autofluorescence (AF) imaging was performed at both three and five months of age. Compared to controls, IR imaging in the *Cln7* KO mice displayed vasculature attenuation and hyperfluorescent regions at three months of age that persisted through five months of age (Fig. 5a). AF imaging displayed hyperfluorescent puncta in the *Cln7* KO mice, but

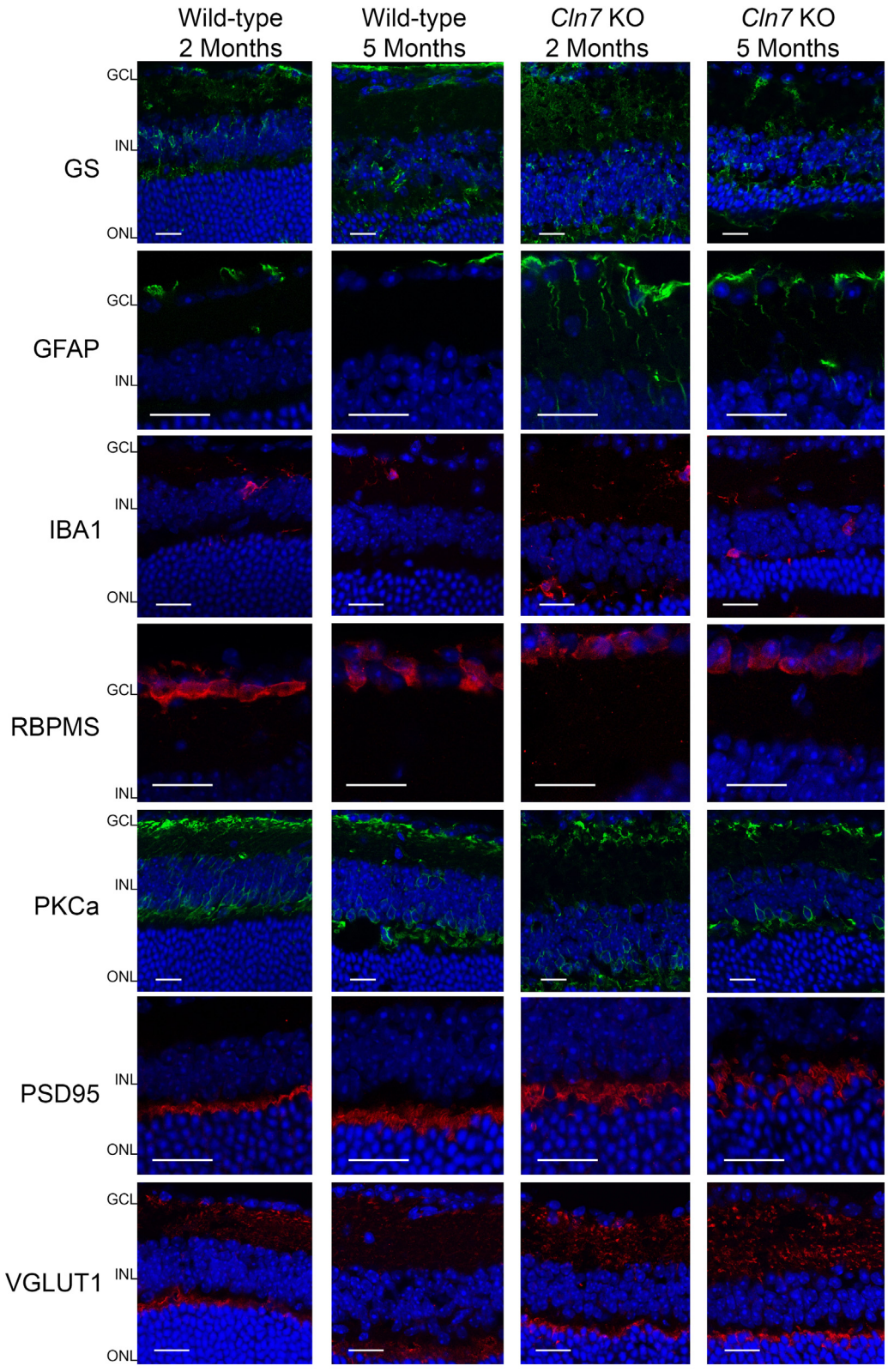
Wild-type
2 Months
Wild-type
5 Months
Cln7 KO
2 Months
Cln7 KO
5 Months
GS
GFAP
IBA1
RBPMS
PKCa
PSD95
VGLUT1
GCL
INL
ONL

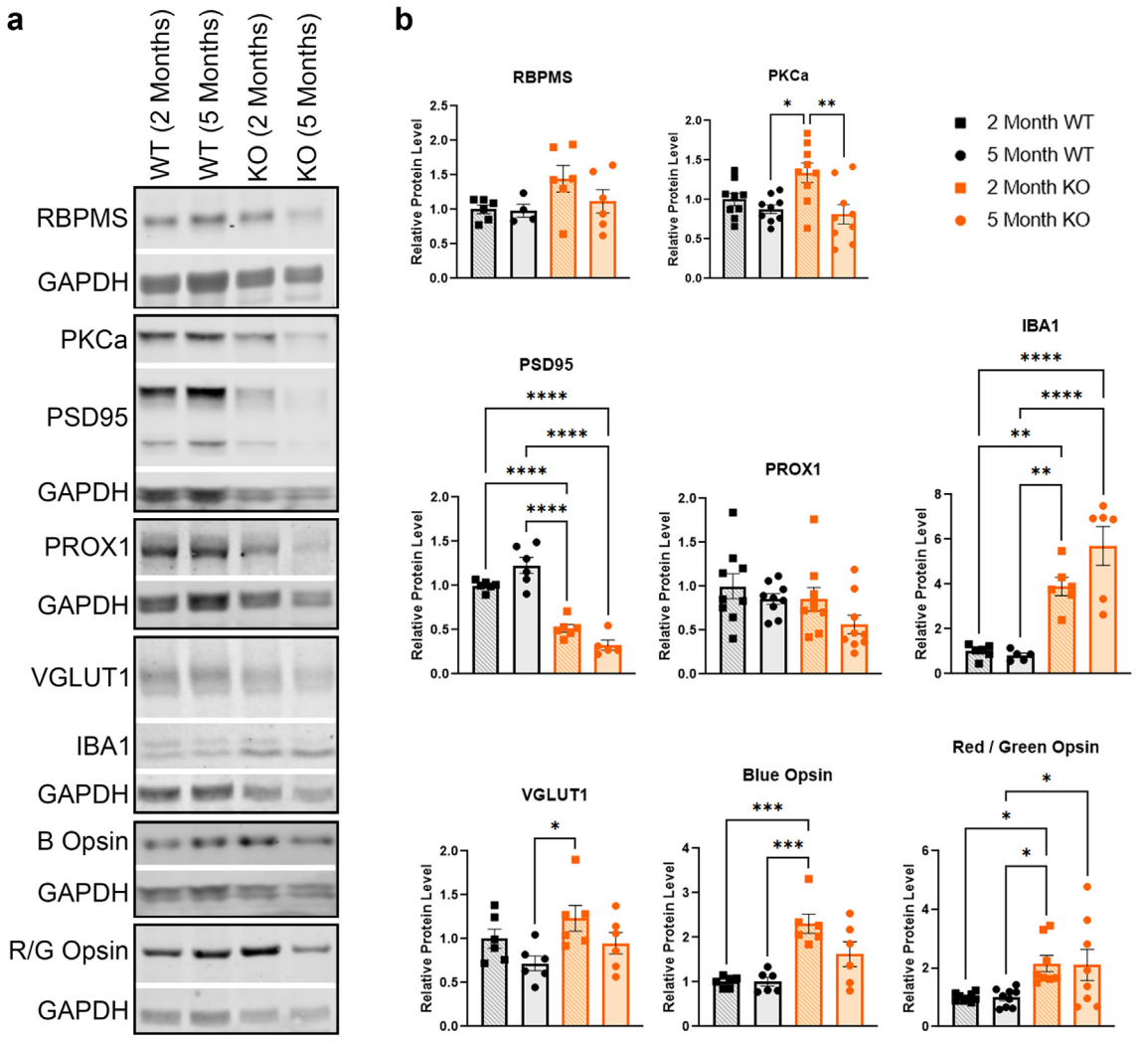

Fig. 4:* Five month old *Cln7* knockout (KO) mice show increased microglial activation and reduced bipolar cells and photoreceptor synapses**. Retinal lysates were collected from eyes of two and five month old wild-type and *Cln7* KO mice. (a) Representative Western blot membrane for RBPMS (RNA binding protein with multiple splicing), PKCα (protein kinase c alpha), PSD95 (post synaptic density protein 95), PROX1 (prospero homeobox 1), VGLUT1 (vesicular glutamine transporter 1), IBA1 (ionized calcium-binding adaptor molecule 1), B Opsin (blue cone opsin), and R/G Opsin (red/green cone opsin) along with respective GAPDH loading controls. (b) Densitometry of the Western blot results. N = three mice per group, two or more technical replicates per mouse per antibody. Error bars = SEM. One-way ANOVA with Tukey's multiple comparisons test. PKCA (*P = 0.013; **P = 0.0038); PSD95 (*P < 0.0001); IBA1 (**P = 0.0032 for comparison to two month wild-type and 0.0028 for comparison to five month wild-type; ****P < 0.0001); VGLUT1 (*P = 0.028); B Opsin (***P = 0.0004); R/G Opsin (*P = 0.039 for comparison to two month wild-type, 0.038 for five month wild-type compared to two month KO, and 0.049 for comparison of five month wild-type and five month KO).

***Fig. 3:* Immunostaining displays glial activation and a reduction in the bipolar cells and photoreceptor synapses by five months of age in the *Cln7* knockout (KO) mouse**. Representative immunostained sections of retinas of two and five month wild-type and *Cln7* KO mice. Staining was performed for GS (glutamine synthetase), GFAP (glial fibrillary acidic protein), IBA1 (ionized calcium-binding adaptor molecule 1), RBPMS (RNA binding protein with multiple splicing), PKCα (protein kinase c alpha), PSD95 (post synaptic density protein 95), and VGLUT1 (vesicular glutamine transporter 1) in either red or green fluorescence. DAPI staining shown in blue. N = three mice per group, at least three retinal sections per eye. Scale bar = 25 μm. GCL, ganglion cell layer; INL, inner nuclear layer; ONL, outer nuclear layer.

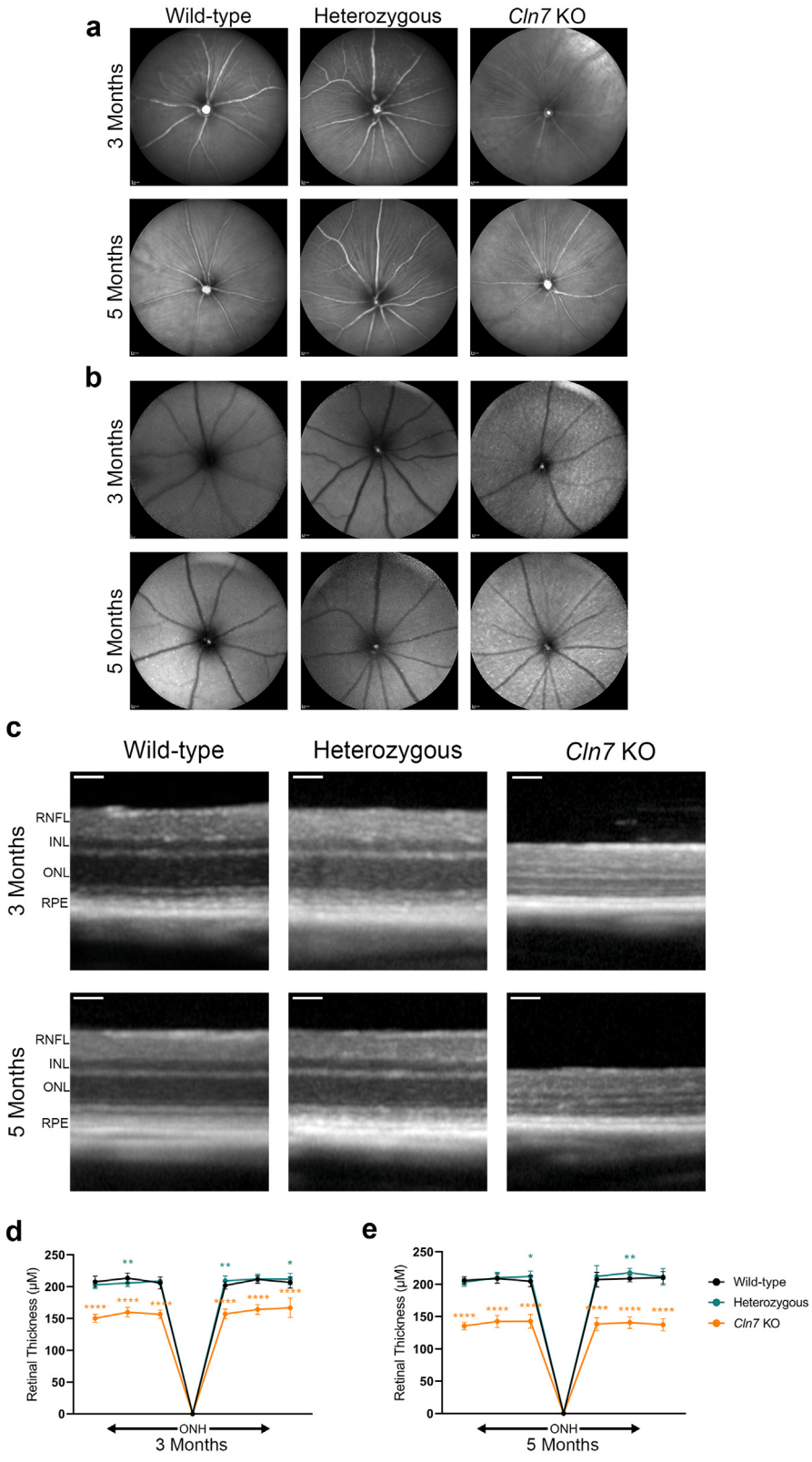
a
Wild-type
Heterozygous
Cln7 KO
3 Months
5 Months
b
3 Months
5 Months
c
Wild-type
Heterozygous
Cln7 KO
3 Months
RNFL
INL
ONL
RPE
5 Months
RNFL
INL
ONL
RPE
d
Retinal Thickness (µM)
250
200
150
100
50
0
ONH
3 Months
e
Retinal Thickness (µM)
250
200
150
100
50
0
ONH
5 Months
Wild-type
Heterozygous
Cln7 KO

not in either control, at three months of age (Fig. 5b). Some wild-type and heterozygous *Cln7* control mice did display some hyperfluorescence at five months of age, likely due to natural aging.

Long-term optical coherence tomography (OCT) displays reduction of the photoreceptors over time

To investigate the retinal degeneration in each cellular layer, we performed OCT imaging at both three and five months of age in the wild-type, *Cln7* heterozygous, and *Cln7* KO mice. Reduced thickness of the retina was detected in the *Cln7* KO mice compared to both controls, with a noticeable loss of the ONL (Fig. 5c). Quantification of the retinal thickness displayed an approximate 20–25% thinning at three months of age (Fig. 5d) [*P = 0.041; **P = 0.0013 and 0.0031; ****P < 0.0001; two-way ANOVA with Tukey's multiple comparisons test] which progressed to an approximate 33% thinning by five months of age (Fig. 5e) [*P = 0.014; **P = 0.0022; ****P < 0.0001; two-way ANOVA with Tukey's multiple comparisons test].

The CLN7 preclinical model shows a progressive loss of visual function, including cones, over time

Since we observed a loss of retinal thickness in the *Cln7* KO mice on OCT analysis, as well as detected signs of photoreceptor degeneration on IR and AF imaging, we then investigated the function of the retinal cells. Scotopic electroretinography (ERG) was performed at post-natal day (P)21 and P28, to examine retinal function early in disease progression. Dim, white light (0.01 cd.s/m^2 flash intensity), ERG traces displayed a loss of the b-wave amplitudes in the *Cln7* KO mice compared to controls at both P21 and P28, indicating reduced function of the rod photoreceptor cells (Fig. 6a, b). Quantification of dim-light, scotopic ERG amplitudes confirmed the results seen in the representative traces, where the *Cln7* KO mice displayed a significant loss of the b-wave at P21 (143 μV compared to 275 μV for the control) and P28 (113 μV compared to 374 μV for the control; Fig. 6c) [**P = 0.0027; ****P < 0.0001; two-way ANOVA with Šidák's multiple comparisons test]. At bright light (1.0 cd.s/m^2 flash intensity), ERG traces displayed a loss of both the a- and b-wave amplitudes in the *Cln7* KO mice compared to controls at both P21 and P28, indicating reduced function of the neural retina (Fig. 6d, e). Quantification of bright-light, scotopic ERG amplitudes confirmed the results seen in the representative traces, where the *Cln7* KO mice displayed a significant loss of the a-wave at P21 (–127 μV compared to –251μV for the control) and P28 (–71 μV compared to –268μV for the control; Fig. 6f) [P < 0.0001; two-way ANOVA with Šidák's multiple comparisons test]. The *Cln7* KO mice displayed a significant loss of the b-wave at P21 (270 μV compared to 518 μV for the control) and P28 (223 μV compared to 561 μV for the control; Fig. 6g) [P < 0.0001; two-way ANOVA with Šidák's multiple comparisons test].

To follow the natural progression of retinal function loss, scotopic ERG was performed at two, four, and six months of age in the wild-type, *Cln7* heterozygous, and *Cln7* KO mice. Scotopic ERG traces displayed a loss of both the a- and b-wave amplitudes in the *Cln7* KO mice compared to controls at two months of age (Fig. 7a). Both the a- and b-wave amplitudes continued to degenerate in the *Cln7* KO mice at four (Fig. 7b) and six months of age (Fig. 7c), with *Cln7* heterozygous mice remaining similar to wild-type throughout the six month analysis. Quantification of scotopic ERG amplitudes confirmed the results seen in the representative traces, where the *Cln7* KO mice displayed a significant loss of the a-wave (–45 μV compared to approximately –150μV for both control groups) at two months of age (Fig. 7d) [P < 0.0001; one-way ANOVA with Tukey's multiple comparisons test]. This decline continued to be significant at both four (–22 μV; Fig. 7e) and six (–16.13 μV; Fig. 7f) months of age [P < 0.0001; one-way ANOVA with Tukey's multiple comparisons test]. Additionally, the a-wave amplitude significantly declined within the *Cln7* KO mouse cohort over the six months, providing insight into the natural progression of retinal degeneration in CLN7 Batten disease (Fig. 7m) [**P = 0.0042; ***P = 0.0003; one-way ANOVA with Tukey's multiple comparisons test]. Investigation of the b-wave displayed similar results to that noted for the a-wave (Fig. 7g–i). *Cln7* KO mice showed a significant reduction in b-wave amplitudes at all times analysed (approximately 166.54 μV, 127.73 μV, and 58.11 μV compared to approximately 305.38 μV for both controls) [**P = 0.0012 compared to wild-type and P = 0.0033 compared to heterozygous mice; ****P < 0.0001; one-way ANOVA with Tukey's multiple comparisons test]. The *Cln7* KO preclinical model also

Fig. 5: **Long-term live imaging indicates progressive photoreceptor cell degeneration in the *Cln7* KO mice.** Representative images for wild-type, *Cln7* heterozygous and *Cln7* KO mice (left, middle, and right, respectively) at three and five months of age for (a) infrared (IR) scanning laser ophthalmoscope (SLO) and (b) blue autofluorescence SLO. (c) Representative OCT images for wild-type, *Cln7* heterozygous and *Cln7* KO mice (left, middle, and right, respectively) at three and five months of age. Spider plot quantification of the retinal thickness, measured at six regions of the OCT image for wild-type, *Cln7* heterozygous and *Cln7* KO mice (black, teal, and orange, respectively) at three (d) and five (e) months of age. RNFL, retinal nerve fiber layer; INL, inner nuclear layer; ONL, outer nuclear layer; RPE, retinal pigmented epithelium; ONH, optic nerve head. N ≥ five mice per group. Scale bar = 200 μm. Error bars = SD. Two-way ANOVA with Tukey's multiple comparisons test. Three months (*P = 0.041; **P = 0.0013 and 0.0031; ****P < 0.0001) and five months (*P = 0.014; **P = 0.0022; ****P < 0.0001).

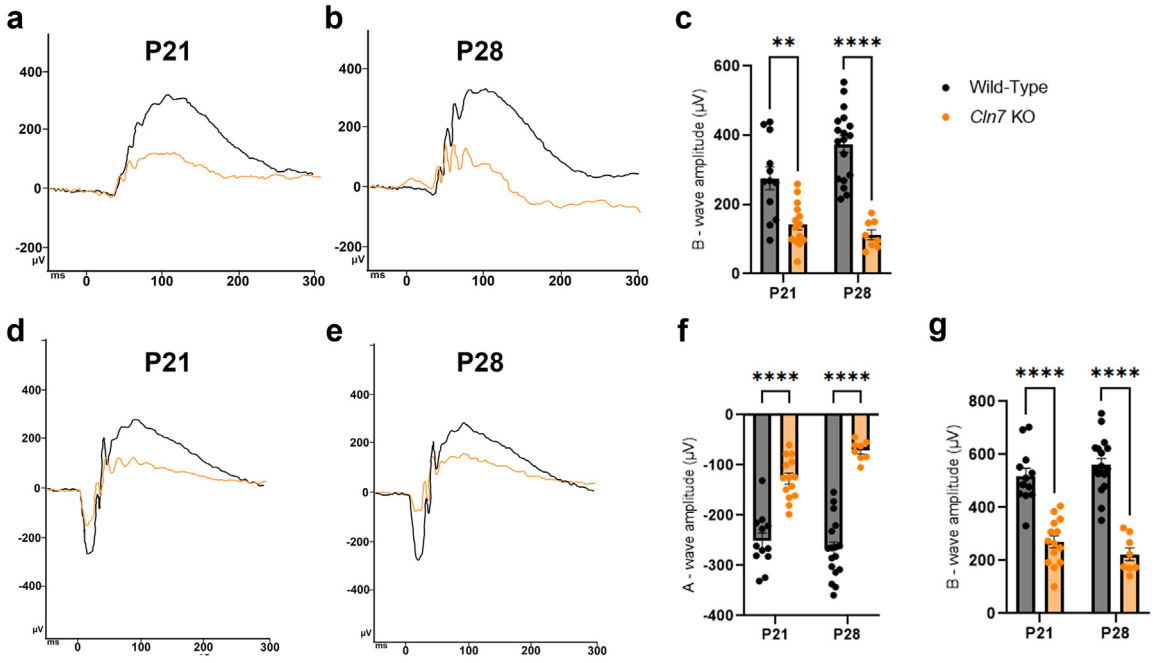

Fig. 6: **The CLN7 preclinical model shows a progressive loss of visual function prior to one month of age**. Representative low-light (0.01 cd.s/m^2 flash intensity) scotopic electroretinography (ERG) traces for wild-type (black) and *Cln7* knockout (KO; orange) mice at (a) post-natal day (P)21 and (b) P28. (c) ERG b-wave maximal amplitudes at P21 and P28 for the low-light scotopic ERG. Representative bright-light (1.0 cd.s/m^2 flash intensity) scotopic ERG traces for wild-type (black) and *Cln7* knockout (KO; orange) mice at (d) P21 and (e) P28. (f) ERG a-wave maximal amplitudes and (g) b-wave maximal amplitudes at P21 and P28 for the bright-light scotopic ERG. Y-axis is in μV. N ≥ eight eyes per group. Error bars = SEM. Two-way ANOVA with Šidák's multiple comparisons test. **P = 0.0027; ****P < 0.0001.

displayed a statistically significant decline in b-wave amplitudes over six months (Fig. 7n) [*P = 0.014; ****P < 0.0001; one-way ANOVA with Tukey's multiple comparisons test].

Since we found a reduction in the INL by six months of age in the *Cln7* KO mice on histological analysis, and an indication of this loss at five months of age by protein analysis, we tested whether or not the INL signalling was compromised over time. We found that the oscillatory potentials (OPs) were similar between the *Cln7* KO mice and control groups at two months of age [*P = 0.0495 and 0.034 for P5; two-way ANOVA with Tukey's multiple comparisons test], but that the OPs significantly declined by four months of age (Fig. 7j and k) [*P = 0.033 for P3 and P = 0.011 for P5; **P = 0.0098; ***P = 0.0002; two-way ANOVA with Tukey's multiple comparisons test] and continued to significantly decline through six months (Fig. 7l) [*P = 0.044; ****P < 0.0001; two-way ANOVA with Tukey's multiple comparisons test].

As the *Cln7* KO mice displayed indications of photoreceptor degeneration on histology and clinical imaging, we examined the function of the individual photoreceptors. Dim, green-light, scotopic ERGs were used to examine rod function at two, four and six months of age. At two months of age, rod function at this light setting was similar between the *Cln7* KO mice and their controls (Fig. 8a, d) [P = 0.022 between wild-type and *Cln7* heterozygous mice; one-way ANOVA with Tukey's multiple comparisons test]. However, a significant reduction in the rod ERG response was detected by four months of age (86.83 μV compared to approximately 149.8 μV for both controls; Fig. 8b, e) [*P = 0.029; **P = 0.002; one-way ANOVA with Tukey's multiple comparisons test] and at six months of age (41.63 μV compared to approximately 206.65 μV for both controls; Fig. 8c, f) [P < 0.0001; one-way ANOVA with Tukey's multiple comparisons test]. Rod function significantly declined over the six month analysis within the *Cln7* KO cohort (Fig. 8g) [**P = 0.0084; ****P < 0.0001; one-way ANOVA with Tukey's multiple comparisons test].

Previous reports did not note cone degeneration in the *Cln7* KO mice, but analysis was halted by four months of age.[7] Since we found that rod function declined over time, and photoreceptor degeneration was shown to progress through our six month analysis, we hypothesized that cone degeneration may be detectable after four months of age. To test this hypothesis, we looked at cone function using flash and flicker photopic ERG at early-stage disease (P21 and P28) as well as late-

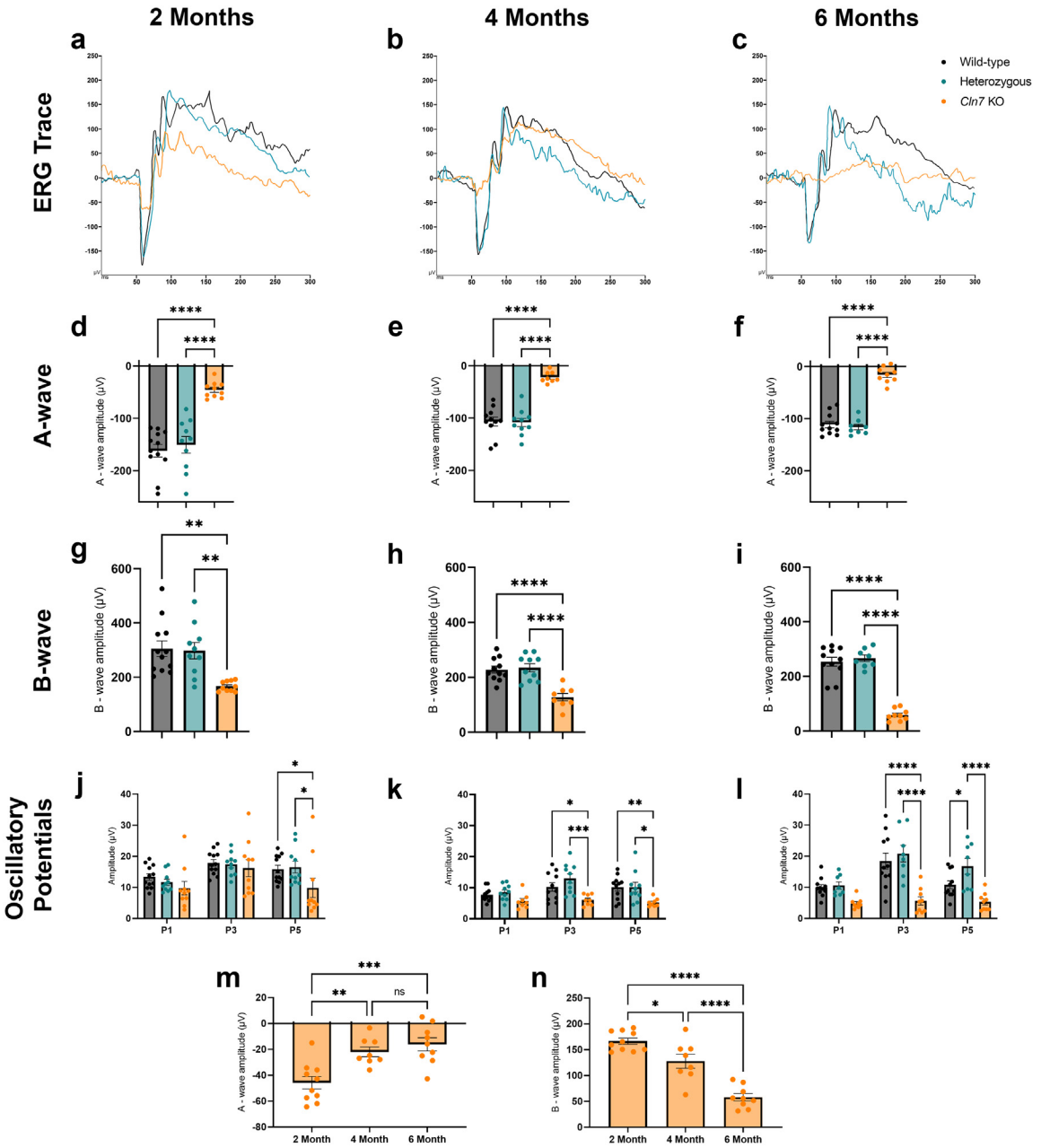

Fig. 7: **The CLN7 preclinical model shows a progressive loss of visual function over time**. Representative scotopic electroretinography (ERG) traces for wild-type (black), *Cln7* heterozygous (teal) and *Cln7* knockout (KO; orange) mice at (a) two, (b) four, and (c) 6 months of age. Y-axis is in μV. (d–f) ERG a-wave, (g–i) b-wave, and (j–l) oscillatory potential (OP) responses in wild-type, *Cln7* heterozygous and *Cln7* KO mice at (d, g, j) two, (e, h, k) four, and (f, i, l) six months of age. A-wave and b-wave ERGs were analysed with one-way ANOVA with Tukey's multiple comparisons test; OPs were analysed with two-way ANOVA with Tukey's multiple comparisons test. A-wave (****P < 0.0001); b-wave (**P = 0.0012 compared to wild-type and P = 0.0033 compared to heterozygous mice); Two month OPs (*P = 0.0495 and 0.034 for P5); Four month OPs (*P = 0.033 for P3 and P = 0.011 for P5; **P = 0.0098; ***P = 0.0002); Six month OPs (*P = 0.044; ****P < 0.0001). ERGs for the *Cln7* KO mice over time for the (m) a-wave and (n) b-wave. A-wave (**P = 0.0042; ***P = 0.0003); B-wave (*P = 0.014; ****P < 0.0001). All ERG measurements were recorded at a 2.5 log cd.s/m^2 flash intensity setting and measured in μV. N≥ eight eyes per group. Error bars = SEM.

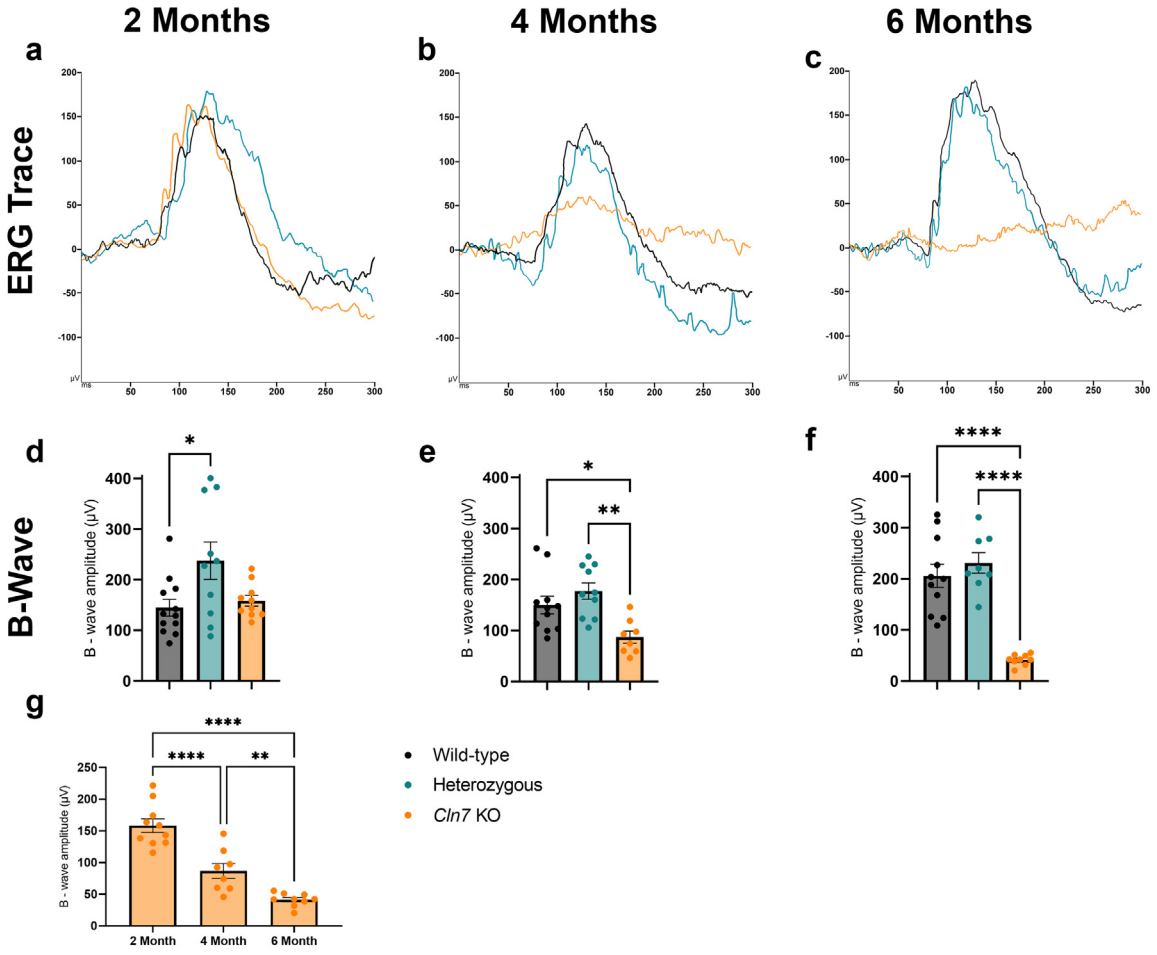

Fig. 8: **The CLN7 preclinical model shows a progressive loss of rod photoreceptor function over time**. Representative scotopic electroretinography (ERG) traces for wild-type (black), *Cln7* heterozygous (teal) and *Cln7* knockout (KO; orange) mice at (a) two, (b) four, and (c) 6 months of age. Y-axis is in μV. ERG b-wave responses in wild-type, *Cln7* heterozygous and *Cln7* KO mice at (d) two, (e) four, and (f) six months of age. One-way ANOVA with Tukey's multiple comparisons test. Two month (*P = 0.022); Four month (*P = 0.029; **P = 0.002); Six month (****P < 0.0001). (g) ERGs for the *Cln7* KO mice over time for the b-wave amplitude. **P = 0.0084; ****P < 0.0001. All ERG measurements were recorded at a −1.1 log cd.s/m^2 flash intensity setting and measured in μV. N ≥ eight eyes per group. Error bars = SEM.

stage disease (five months of age) in wild-type and *Cln7* KO mice. Surprisingly, we found that flash photopic ERG responses were significantly decreased in the early-stage *Cln7* KO mice examined with 10.0 Hz light intensity (69 μV for the *Cln7* KO mice compared to 116 μV for controls at P21, and 58 μV for the *Cln7* KO mice compared to 114 μV for controls at P28; Fig. 9a, c) [P = 0.0006 at P21 and P = 0.0002 at P28; two-way ANOVA with Tukey's multiple comparisons test]. Flicker photopic ERG responses showed a similar trend, with a significant reduction in the *Cln7* KO mice compared to wild-type controls at a 30.0 Hz light intensity beginning at P28 (9 μV for the *Cln7* KO mice compared to 13 μV for controls at P21, and 5 μV for the *Cln7* KO mice compared to 21 μV for controls at P28; Fig. 9b, e) [P = 0.0051; two-way ANOVA with Tukey's multiple comparisons test].

At late-stage of disease, we found that flash photopic ERG responses were significantly decreased in the *Cln7* KO mice (25.37 μV for the *Cln7* KO mice compared to 55.82 μV for controls at 3.0 Hz light intensity, and 34.75 μV for the *Cln7* KO mice compared to 92.64 μV for controls at 10.0 Hz light intensity; Fig. 9a, d) [P < 0.0001; unpaired student's *t*-test]. Flicker photopic ERG responses showed a similar trend, with a significant reduction in the *Cln7* KO mice compared to wild-type controls (4.96 μV for the *Cln7* KO mice compared to 33.95 μV for controls at 10.0 Hz light intensity, and 3.53 μV for the *Cln7* KO mice compared to 6.33 μV for controls at 30.0 Hz light intensity; Fig. 9b, f) [*P = 0.028; ***P = 0.0004; unpaired student's *t*-test].

As we detected a loss of cone function before one month of age but it persisted through at least five months of age, we examined the retinas of *Cln7* KO

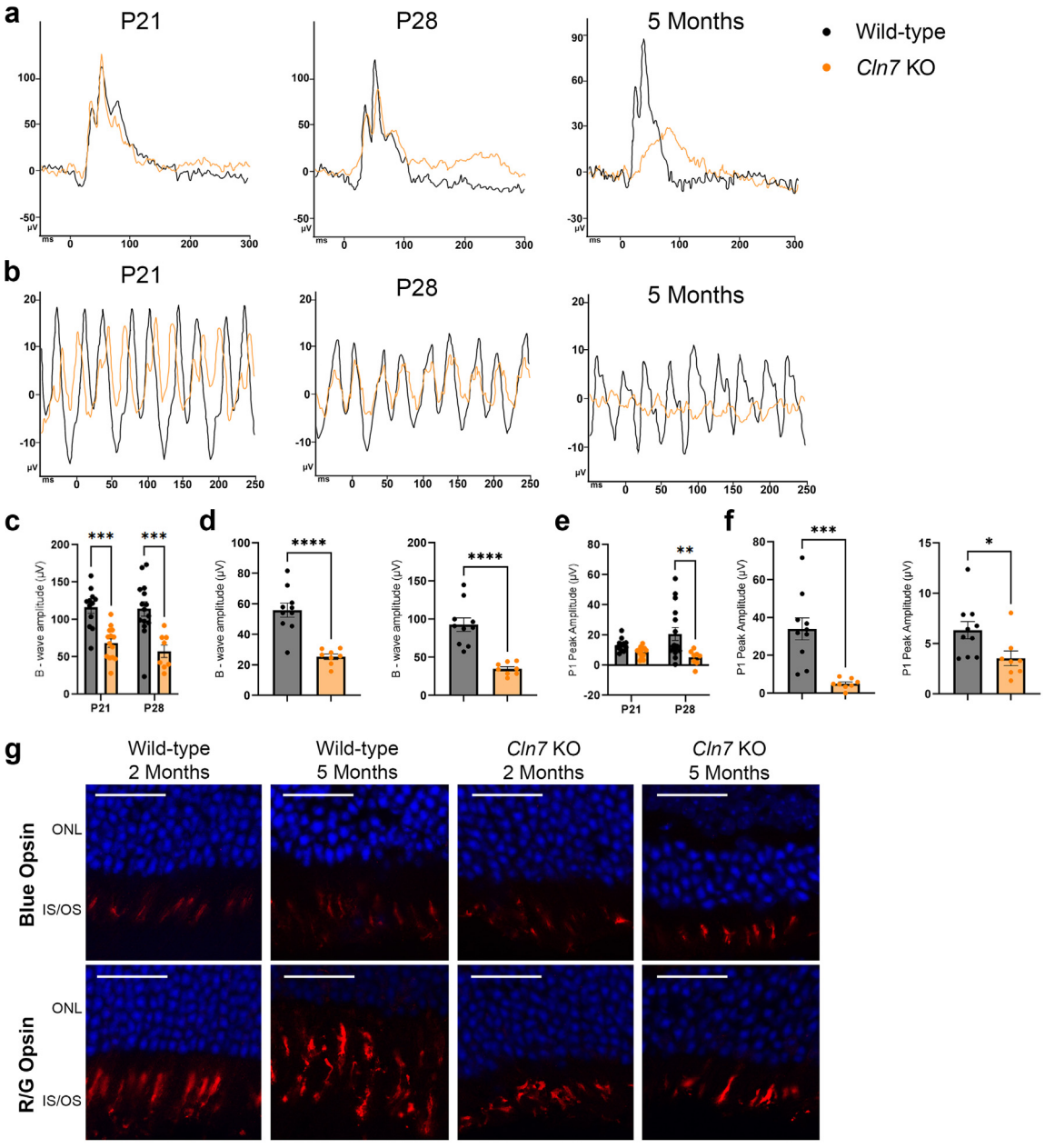

Fig. 9:* The CLN7 preclinical model shows a loss of cone photoreceptor function before one month of age**. Representative photopic electroretinography (ERG) traces for wild-type (black) and *Cln7* knockout (KO; orange) mice at post-natal day (P)21, P28 and five months of age. (a) 10.0 Hz light intensity setting and (b) 30.0 Hz flicker response. Photopic ERG amplitudes were compared between wild-type and *Cln7* KO mice for (c) 10.0 Hz photopic at P21 and P28, (d) 3.0 Hz photopic and 10.0 Hz photopic at five months, (e) 30.0 Hz flicker at P21 and P28, and (f) 10.0 Hz and 30.0 Hz flicker at five months. ERG recordings were measured in µV. N ≥ eight eyes per group. Error bars = SEM. P21 and P28 data were analysed with two-way ANOVA with Tukey's multiple comparisons test. Five month data were analysed with unpaired student's *t*-test. Flash photopic ERG (P = 0.0006 at P21 and P = 0.0002 at P28; ****P < 0.0001); Flicker ERG (*P = 0.028; **P = 0.0051; ***P = 0.0004). (g) Immunostaining of two and five month wild-type and *Cln7* KO mouse retinas for Blue Opsin (top panels) and Red/Green (R/G) Opsin (bottom panels). DAPI staining in blue. Scale Bar = 25 µm. N = three mice per group and at least three retinal sections per eye. ONL, outer nuclear layer; IS/OS, inner segment/outer segment.

mice for cones at both two and five months of age. Blue opsin staining was present in the *Cln7* KO retinas, but displayed a collapsed morphology compared to wild-type controls (Figs. 9g and S5). Upon analysis of red/green opsin, the *Cln7* KO mice also showed the collapsed morphology (Fig. 9g; Fig. S5). Protein analysis in the *Cln7* KO retinas showed a significant elevation of both blue opsin [P = 0.0004; one-way ANOVA with Tukey's multiple comparisons test] and red/green opsin [P = 0.039 for comparison to two month wild-type, 0.038 for five month wild-type compared to two month KO, and 0.049 for comparison of five month wild-type and five month KO; one-way ANOVA with Tukey's multiple comparisons test] compared to wild-type controls, possibly reflecting a larger portion of cone protein when rods are lost in the *Cln7* KO retinas (Fig. 4).

The *Cln7* KO mice display a significant loss of visual function within the retinal network

Since CLN7 Batten disease leads to neuronal degeneration in the brain as well as retina, we hypothesized that downstream visual processing will be affected in the *Cln7* KO preclinical model. To test this hypothesis, we performed pattern ERG (PERG) on the *Cln7* KO mice and wild-type controls at five months of age. The PERG waveform was normal but significantly reduced in the *Cln7* KO mice, indicating transmission defects in ganglion cells (Fig. S6a, c) [P = 0.023; unpaired student's *t*-test]. We also tested pattern visually evoked potentials (VEPs) and found that these were reduced but not significantly altered in the *Cln7* KO mice (Fig. S6b, d) [Unpaired student's *t*-test].

The *Cln7* KO mice exhibit reduced sensitivity toward intraperitoneally (IP) delivered anaesthetics

A loss of *Mfsd8* causes lysosomal dysfunction, and it is likely to impact the degradation and metabolism of various compounds.[30,31] In our study, we found that wild-type, *Cln7* heterozygous, and *Cln7* KO mice had similar body weights (in grams), respective of their sex and age (Fig. 10a, b) [two-way ANOVA with Tukey's multiple comparisons test]. However, we discovered that the *Cln7* KO mice required significantly greater doses of ketamine anaesthetic in order to undergo clinical imaging, and that this requirement increased over time to levels that were lethal in wild-type and *Cln7* heterozygous mice (Fig. 10c) [**P = 0.0049 compared to wild-type and P = 0.0086 compared to heterozygous mice; ****P < 0.0001; two-way ANOVA with Tukey's multiple comparisons test]. At two months of age, the *Cln7* KO mice required approximately 116% of the amount of ketamine per body weight required for the control mice. By six months of age, this level had increased to be 144% of the age-matched controls. Although these mice required heavy dosage of IP anaesthetic to undergo clinical imaging, no adverse complications were detected and all mice recovered normally.

Discussion

Batten disease is a fast-progressing, paediatric condition characterized by impaired vision, seizures, loss of motor control and premature death.[1] The ability to use gene therapy advances to treat patients is promising. However, there remains a need to understand the natural progression of retinal degeneration in these patients in order to define clinical therapeutic outcomes and efficacy to treat vision loss. For instance, the ability to gather natural history information on vision loss was critical for setting the baselines for therapeutic efficacy in the gene therapy clinical trials for Leber Congenital Amaurosis (LCA) caused by mutations in *RPE65*, which led to the first Food and Drug Administration-approved *in vivo* gene therapy.[32] Studies investigating human patients and mammalian models for this early-onset childhood retinal degenerative disease found that ERGs were reduced or non-detectable at early ages, indicating that therapeutic intervention is necessary at an early stage of disease.[33–36]

In this study, we performed visual examinations on five patients with CLN7 Batten disease. Although this is a cohort with a small sample size, data obtained showed that these patients were far progressed in retinal degeneration within their first five years of life. This is expected to represent the general population of CLN7 patients, as the disease presents within the late-infantile age with an early retinal degenerative phenotype. We did find that the youngest patient displayed an electronegative ERG with reduced, but present, a-waves OU. This indicates the possibility of an early photoreceptor to bipolar synaptic defect. However, there was no ERG data collected at this earlier age for the other four patients, and it may be an outcome specific to this single case, and not CLN7 Batten disease patients as a whole.

Other mammalian models for the study of NCLs have provided insight into the mechanisms underlying retinal degeneration.[37–41] For instance, the retinal degeneration noted in the $Cln3^{\Delta ex7/8}$ mouse model for CLN3 Batten disease displays a loss of the bipolar cells, and this can be rescued using gene therapy approaches targeting the bipolar cells.[42] Surprisingly, in the $Cln6^{nclf}$ mouse model of CLN6 Batten disease, the main retinal cell loss is in the photoreceptors, similar to that shown in the CLN7 mouse model.[38] However, gene therapy vectors targeting the photoreceptor cells were unable to delay retinal degeneration in the $Cln6^{nclf}$ mouse, but vectors that targeted the bipolar cells delayed photoreceptor degeneration.[43] This indicates a possible critical role for the bipolar cells in preserving retinal function in Batten disease.

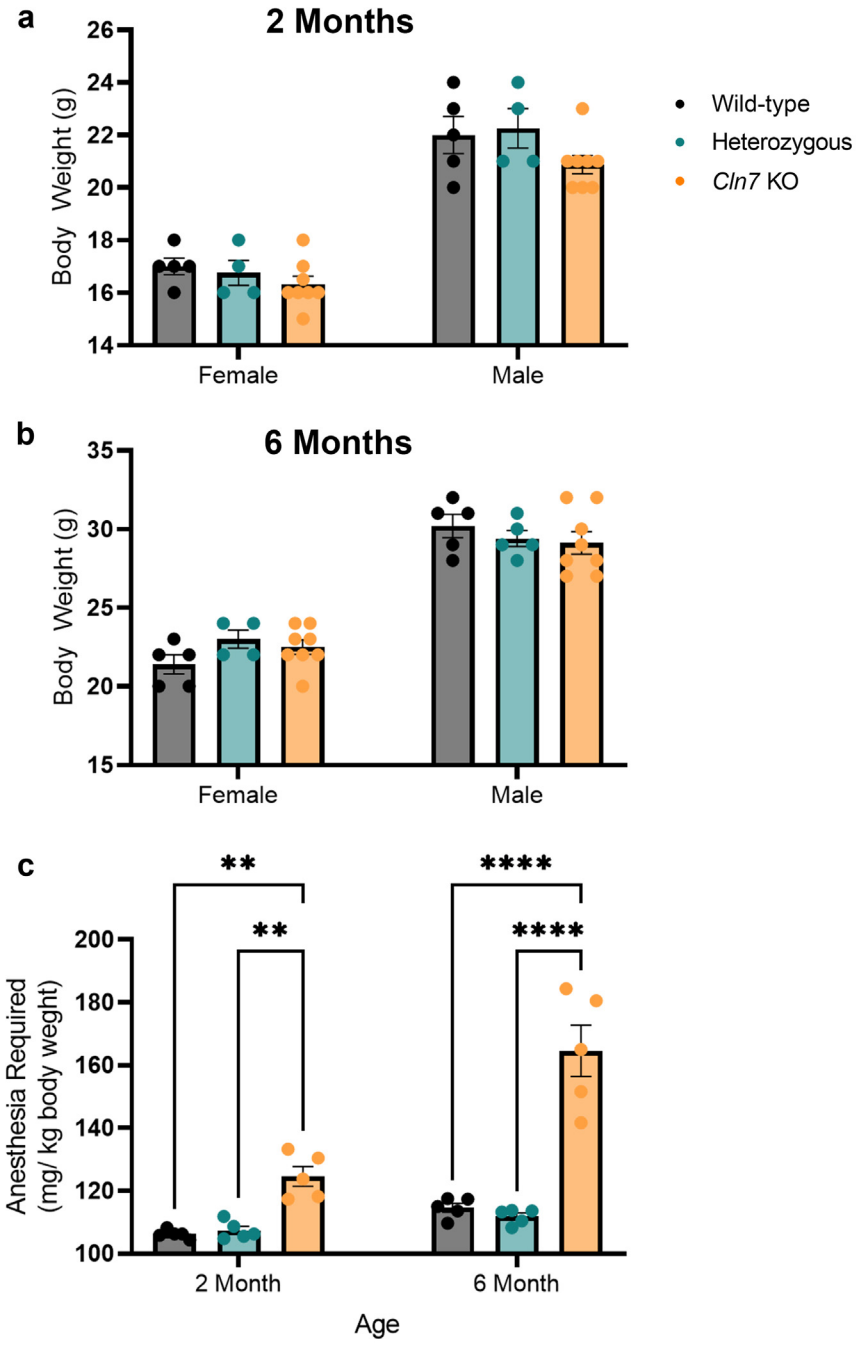

Fig. 10: **The CLN7 knockout (KO) mice exhibit reduced sensitivity toward intraperitoneally (IP) delivered anaesthetics**. The body weight in grams of wild-type (black), *Cln7* heterozygous (teal), and *Cln7* KO (orange) mice was recorded prior to anesthetized events at (a) two months and (b) six months of age, separated by gender. (c) Anaesthesia administered via IP injection was recorded in mg/kg body weight at two and six months of age. N = five mice per group. Error bars = SEM. Two-way ANOVA with Tukey's multiple comparisons test. **P = 0.0049 compared to wild-type and P = 0.0086 compared to heterozygous mice; ****P < 0.0001.

To further investigate the progression of retinal degeneration during CLN7 Batten disease, we utilized the *Cln7* KO mouse model.[19,20] This model has its limitations as the neurological deficits arise much later than seen in human patients.[19] However, retinal degeneration was noted in this preclinical model before one month of age, similar to human patients. No clinical imaging had been performed and no analysis beyond four months of age was carried out for the *Cln7* KO mice.[18] In our study, we followed this preclinical model of CLN7 Batten disease through six months of age, the time in which the mice present with seizures, paralysis and premature death.[20] We not only found a rapid rod degeneration as previously shown,[18] but a significant loss of cone photoreceptor function before one month of age, although the cells persisted over time. This ability to monitor both rod and cone survival and function over time provides a baseline for testing the efficacy of potential clinical therapeutics on the photoreceptor cells and visual preservation.

Furthermore, human CLN7 Batten disease patients show a loss of the bipolar cells of the inner nuclear layer (INL), which has not been previously detected in the *Cln7* KO mouse.[18] In our study, we detected a significant loss of the INL on histological analysis at six months of age, and found that beginning at four months of age there was a significant and progressive decline in the oscillatory potentials. These indicate signalling loss in the inhibitory amacrine and bipolar cells. Immunostaining analysis showed a possible reduction in VGLUT1 in the outer plexiform layer (OPL) at two months of age, suggestive of a defect in photoreceptor to bipolar synaptic signalling. Protein analysis of VGLUT1 did not show a reduction in the *Cln7* KO mice at five months of age, but this may be due to the fact that it detected both VGLUT1 in the IPL and OPL, and the change visible on immunostaining in the OPL was not drastic enough to detect with Western blot of whole retinas. There was a similar trend for the bipolar cells, where a reduction was visible by immunostaining at five months of age in the *Cln7* KO mice, but this was significant on Western blot analysis only between early- and late-stage *Cln7* KO mice, and not when compared to wild-type controls. We did find variability in the rate of degeneration within *Cln7* KO mice over time, with some progressing to a significant loss of the ONL and INL by five months of age, while others required six months or longer to show a significant reduction in the INL.

In our study, we examined single dependent variables (i.e. scotopic visual response, outer nuclear layer thickness, etc.). There is a potential for confounding variables to play a role on the variables examined in this study. For instance, the cage location within the animal facility where the mice are housed as well as the nesting and social arrangement of the mice within a single cage can impact the light exposure to a given mouse, possibly affecting the rate of retinal degeneration. Additionally, the precise time of day for experimental methods, such as ERG, can play a role in the electrical response obtained. To reduce the likelihood of these confounding factors, we housed our mice in the same row and rack of the same animal facility room, as well as performed ERGs on controls and experimental littermates on the same day and same window of time (morning or afternoon).

All of this data opens up the possibility that early in CLN7 Batten disease, defects arise in the synaptic connections to the bipolar cells. These would likely occur prior to the onset of rod and cone functional loss, followed by rod degeneration and secondary death of the cones with a late-onset degeneration of the INL, likely the bipolar cells. As mentioned, recent gene therapy approaches in a preclinical model of CLN6 Batten disease - also caused by a loss of the rod photoreceptors - determined that targeting the bipolar cells was necessary for therapeutic efficacy.[7] Future studies are needed to test gene therapy vectors targeted specifically to either photoreceptor or bipolar cells using this *Cln7* KO mouse model.

One surprising outcome of our study was the sensitivity to intraperitoneally (IP) injected anaesthetics. Cerebral and retinal impaired lysosomal function has been shown in *Cln7* KO mice,[30,31,44–46] which can impact the ability to metabolize drug compounds. We find that care should be taken in treatment of human CLN7 Batten disease patients when prescribing drugs or considering anaesthetic options and routes of delivery. Additionally, lysosomal function is known to be important in controlling autophagy pathways in the retina and has implications in the progression of age-related macular degeneration (AMD).[47] Some compound heterozygous CLN7 Batten disease patients present with non-syndromic retinal dystrophies, with the most common presentation that of macular dystrophy with central cone involvement.[7] We found that our *Cln7* KO mouse model has an early loss of cone function, supporting its involvement in macular dystrophy. CLN7 has also recently been found to function as an endolysosomal chloride channel, potentially playing a role in chloride permeability and regulation of lysosomal function in the cell.[48] Future experiments can explore the potential link between CLN7 lysosomal dysfunction and macular degeneration.

Overall, we provide a natural history of retinal degeneration in the preclinical model for CLN7 Batten disease, and define clinical indicators for testing therapeutic outcomes. We found that this preclinical model mimics the human patient retinal disease progression, with a rod-cone dystrophy followed by a late loss of the bipolar cells. Thus, this preclinical model can be followed with clinical imaging to test the efficiency and efficacy of therapeutics to treat retinal degeneration in CLN7 Batten disease.

Contributors

XC, SJG and KJW conceived and designed the study. AAR, XC, ERN, TD, YH, SM, and SNK acquired the data. AAR, XC, and YI provided statistical analyses. AAR and KJW analysed and interpreted the data. AAR and KJW drafted the manuscript. SJG and KJW obtained funding. SJG and KJW supervised the study. AAR and KJW verified the underlying data. All authors had full access to the data in the study and have read and approved the final version of the manuscript.

Data sharing statement

All data associated with this study are present in the paper or in the Supplementary Materials.

Declaration of interests

Ms. Rowe has nothing to disclose. Dr. Chen has nothing to disclose. Ms. Nettesheim has nothing to disclose. Mr. Issioui has nothing to disclose. Dr. Dong has nothing to disclose. Ms. Hu has nothing to disclose. Dr. Messahel has nothing to disclose. Dr. Kayani has nothing to disclose. Dr. Gray has nothing to disclose. Dr. Wert has nothing to disclose.

Acknowledgements

We thank the members of the Department of Ophthalmology at UT Southwestern Medical Center for their advice and discussions. Ms. Nettesheim is supported by NIH grant 5T32GM131945-03. Partial support for the project was provided by a kind gift to Dr. Gray from the Morton Fichtenbaum Charitable Trust. Dr. Wert is supported by funds from the Van Sickle Family Foundation Inc. of Dallas, TX. The Department of Ophthalmology at UT Southwestern Medical Center is supported by NIH grant P30 EY030413.

Appendix A. Supplementary data

Supplementary data related to this article can be found at https://doi.org/10.1016/j.ebiom.2022.104314.

References

1 Nita DA, Mole SE, Minassian BA. Neuronal ceroid lipofuscinoses. *Epileptic Disord*. 2016;18(S2):73–88.
2 Chang CH. Neuronal ceroid lipofuscinoses. https://emedicine.medscape.com/article/1178391-overview; 2017. Accessed August 3, 2022.
3 Mink JW, Augustine EF, Adams HR, Marshall FJ, Kwon JM. Classification and natural history of the neuronal ceroid lipofuscinoses. *J Child Neurol*. 2013;28(9):1101–1105.
4 Wisniewski KE, Kida E, Golabek AA, Kaczmarski W, Connell F, Zhong N. Neuronal ceroid lipofuscinoses: classification and diagnosis. *Adv Genet*. 2001;45:1–34.
5 Wisniewski KE, Zhong N, Philippart M. Pheno/genotypic correlations of neuronal ceroid lipofuscinoses. *Neurology*. 2001;57(4):576–581.
6 Cárcel-Trullols J, Kovács AD, Pearce DA. Cell biology of the NCL proteins: what they do and don't do. *Biochim Biophys Acta*. 2015;1852(10 Pt B):2242–2255.
7 Khan KN, El-Asrag ME, Ku CA, et al. Specific alleles of CLN7/MFSD8, a protein that localizes to photoreceptor synaptic terminals, cause a spectrum of nonsyndromic retinal dystrophy. *Invest Ophthalmol Vis Sci*. 2017;58(7):2906–2914.
8 Bartsch U, Storch S. Experimental therapeutic approaches for the treatment of retinal pathology in neuronal ceroid lipofuscinoses. *Front Neurol*. 2022;13:866983.
9 Kohlschutter A, Schulz A, Bartsch U, Storch S. Current and emerging treatment strategies for neuronal ceroid lipofuscinoses. *CNS Drugs*. 2019;33(4):315–325.
10 Craven CL, Gissen P, Bower R, Lee L, Aquilina K, Thompson DNP. A survival analysis of ventricular access devices for delivery of cerliponase alfa. *J Neurosurg Pediatr*. 2022;29(1):115–121.
11 Estublier B, Cano A, Hoebeke C, et al. Cerliponase alfa changes the natural history of children with neuronal ceroid lipofuscinosis type 2: the first French cohort. *Eur J Paediatr Neurol*. 2021;30:17–21.
12 Johnson TB, Cain JT, White KA, Ramirez-Montealegre D, Pearce DA, Weimer JM. Therapeutic landscape for Batten disease: current treatments and future prospects. *Nat Rev Neurol*. 2019;15(3):161–178.
13 Lewis G, Morrill AM, Conway-Allen SL, Kim B. Review of cerliponase alfa: recombinant human enzyme replacement therapy for late-infantile neuronal ceroid lipofuscinosis type 2. *J Child Neurol*. 2020;35(5):348–353.
14 Pharmacoeconomic Review Report: cerliponase Alfa (Brineura). report. In: *Indication: For the Treatment of Neuronal Ceroid Lipofuscinosis Type 2 (Cln2) Disease, Also Known as Tripeptidyl Peptidase 1 (TPP1) Deficiency. CADTH Common Drug Review*; Ottawa (ON): (BioMarin Pharmaceutical (Canada) Inc); 2019.
15 Kousi M, Siintola E, Dvorakova L, et al. Mutations in CLN7/MFSD8 are a common cause of variant late-infantile neuronal ceroid lipofuscinosis. *Brain*. 2009;132(Pt 3):810–819.
16 Mole SE, Cotman SL. Genetics of the neuronal ceroid lipofuscinoses (Batten disease). *Biochim Biophys Acta*. 2015;1852(10 Pt B):2237–2241.
17 MedlinePlus. CLN7 disease. https://medlineplus.gov/genetics/condition/cln7-disease/; 2021. Accessed November 5, 2022.
18 Jankowiak W, Brandenstein L, Dulz S, Hagel C, Storch S, Bartsch U. Retinal degeneration in mice deficient in the lysosomal membrane protein CLN7. *Invest Ophthalmol Vis Sci*. 2016;57(11):4989–4998.
19 Brandenstein L, Schweizer M, Sedlacik J, Fiehler J, Storch S. Lysosomal dysfunction and impaired autophagy in a novel mouse model deficient for the lysosomal membrane protein Cln7. *Hum Mol Genet*. 2016;25(4):777–791.
20 Chen X, Dong T, Hu Y, et al. AAV9/MFSD8 gene therapy is effective in preclinical models of neuronal ceroid lipofuscinosis type 7 disease. *J Clin Invest*. 2022;132(5):e146286.
21 Rowe AA, Patel PD, Gordillo R, Wert KJ. Replenishment of TCA cycle intermediates provides photoreceptor resilience against neurodegeneration during progression of retinitis pigmentosa. *JCI Insight*. 2021;6(17):e150898.
22 Wert KJ, Velez G, Kanchustambham VL, et al. Metabolite therapy guided by liquid biopsy proteomics delays retinal neurodegeneration. *EBioMedicine*. 2020;52:102636.
23 Wert KJ, Bassuk AG, Wu WH, et al. CAPN5 mutation in hereditary uveitis: the R243L mutation increases calpain catalytic activity and triggers intraocular inflammation in a mouse model. *Hum Mol Genet*. 2015;24(16):4584–4598.
24 Wert KJ, Davis RJ, Sancho-Pelluz J, Nishina PM, Tsang SH. Gene therapy provides long-term visual function in a pre-clinical model of retinitis pigmentosa. *Hum Mol Genet*. 2013;22(3):558–567.
25 Wert KJ, Sancho-Pelluz J, Tsang SH. Mid-stage intervention achieves similar efficacy as conventional early-stage treatment using gene therapy in a pre-clinical model of retinitis pigmentosa. *Hum Mol Genet*. 2014;23(2):514–523.
26 Wert KJ, Skeie JM, Bassuk AG, Olivier AK, Tsang SH, Mahajan VB. Functional validation of a human CAPN5 exome variant by lentiviral transduction into mouse retina. *Hum Mol Genet*. 2014;23(10):2665–2677.
27 Fremeau Jr RT, Voglmaier S, Seal RP, Edwards RH. VGLUTs define subsets of excitatory neurons and suggest novel roles for glutamate. *Trends Neurosci*. 2004;27(2):98–103.
28 Johnson J, Tian N, Caywood MS, Reimer RJ, Edwards RH, Copenhagen DR. Vesicular neurotransmitter transporter expression in developing postnatal rodent retina: GABA and glycine precede glutamate. *J Neurosci*. 2003;23(2):518–529.
29 Sherry DM, Wang MM, Bates J, Frishman LJ. Expression of vesicular glutamate transporter 1 in the mouse retina reveals temporal ordering in development of rod vs. cone and ON vs. OFF circuits. *J Comp Neurol*. 2003;465(4):480–498.
30 Kloesel B, Holzman RS. Anesthetic management of patients with inborn errors of metabolism. *Anesth Analg*. 2017;125(3):822–836.
31 Richtsfeld M, Belani KG. Lysosomal storage diseases: past, present, and future. *Anesth Analg*. 2017;125(3):716–718.
32 Acland GM, Aguirre GD, Ray J, et al. Gene therapy restores vision in a canine model of childhood blindness. *Nat Genet*. 2001;28(1):92–95.
33 Al-Khayer K, Hagstrom S, Pauer G, Zegarra H, Sears J, Traboulsi EI. Thirty-year follow-up of a patient with leber congenital

amaurosis and novel RPE65 mutations. *Am J Ophthalmol*. 2004;137(2):375–377.
34 Maeda T, Cideciyan AV, Maeda A, et al. Loss of cone photoreceptors caused by chromophore depletion is partially prevented by the artificial chromophore pro-drug, 9-cis-retinyl acetate. *Hum Mol Genet*. 2009;18(12):2277–2287.
35 Morimura H, Fishman GA, Grover SA, Fulton AB, Berson EL, Dryja TP. Mutations in the RPE65 gene in patients with autosomal recessive retinitis pigmentosa or leber congenital amaurosis. *Proc Natl Acad Sci U S A*. 1998;95(6):3088–3093.
36 Seeliger MW, Grimm C, Stahlberg F, et al. New views on RPE65 deficiency: the rod system is the source of vision in a mouse model of Leber congenital amaurosis. *Nat Genet*. 2001;29(1):70–74.
37 Staropoli JF, Haliw L, Biswas S, et al. Large-scale phenotyping of an accurate genetic mouse model of JNCL identifies novel early pathology outside the central nervous system. *PLoS One*. 2012;7(6):e38310.
38 Bartsch U, Galliciotti G, Jofre GF, Jankowiak W, Hagel C, Braulke T. Apoptotic photoreceptor loss and altered expression of lysosomal proteins in the nclf mouse model of neuronal ceroid lipofuscinosis. *Invest Ophthalmol Vis Sci*. 2013;54(10):6952–6959.
39 Bond M, Holthaus SM, Tammen I, Tear G, Russell C. Use of model organisms for the study of neuronal ceroid lipofuscinosis. *Biochim Biophys Acta*. 2013;1832(11):1842–1865.
40 Shacka JJ. Mouse models of neuronal ceroid lipofuscinoses: useful pre-clinical tools to delineate disease pathophysiology and validate therapeutics. *Brain Res Bull*. 2012;88(1):43–57.
41 Wavre-Shapton ST, Calvi AA, Turmaine M, et al. Photoreceptor phagosome processing defects and disturbed autophagy in retinal pigment epithelium of Cln3Deltaex1-6 mice modelling juvenile neuronal ceroid lipofuscinosis (Batten disease). *Hum Mol Genet*. 2015;24(24):7060–7074.
42 Kleine Holthaus SM, Aristorena M, Maswood R, et al. Gene therapy targeting the inner retina rescues the retinal phenotype in a mouse model of CLN3 Batten disease. *Hum Gene Ther*. 2020;31(13–14):709–718.
43 Kleine Holthaus SM, Ribeiro J, Abelleira-Hervas L, et al. Prevention of photoreceptor cell loss in a Cln6(nclf) mouse model of Batten disease requires CLN6 gene transfer to bipolar cells. *Mol Ther*. 2018;26(5):1343–1353.
44 Gopalakrishnan S, Sidduiqui S, Mayhew JF. Anesthesia in a child with Batten disease. *Paediatr Anaesth*. 2004;14(10):890–891.
45 Lopez-Fabuel I, Garcia-Macia M, Buondelmonte C, et al. Aberrant upregulation of the glycolytic enzyme PFKFB3 in CLN7 neuronal ceroid lipofuscinosis. *Nat Commun*. 2022;13(1):536.
46 Soldati C, Lopez-Fabuel I, Wanderlingh LG, et al. Repurposing of tamoxifen ameliorates CLN3 and CLN7 disease phenotype. *EMBO Mol Med*. 2021;13(10):e13742.
47 Sinha D, Valapala M, Shang P, et al. Lysosomes: regulators of autophagy in the retinal pigmented epithelium. *Exp Eye Res*. 2016;144:46–53.
48 Wang Y, Zeng W, Lin B, et al. CLN7 is an organellar chloride channel regulating lysosomal function. *Sci Adv*. 2021;7(51):eabj9608.